1 **Biological Production in the Indian Ocean Upwelling Zones, Part – I: Refined Estimation**

2 **via the Use of a Variable Compensation Depth in Ocean Carbon Models**

4 Mohanan Geethalekshmi Sreeush[1,2,*].

5 Vinu Valsala[1],

6 Sreenivas Pentakota[1],

7 Koneru Venkata Siva Rama Prasad[2],

8 Raghu Murtugudde[3]

10 [1]Indian Institute of Tropical Meteorology, Pune, India

11 [2]Department of Meteorology and Oceanography, Andhra University, India

12 [3]ESSIC, University of Maryland, USA

14 (*Under revision BGD*)

16 *Corresponding author address:

17 Indian Institute of Tropical Meteorology,

18 Dr. Homi Bhabha Road, Pashan, Pune 411 008, India

19 E-Mail: sreeushmg@tropmet.res.in

Abstract

Biological modeling approach adopted by the Ocean Carbon-cycle Model Inter-comparison Project (OCMIP-II) provided amazingly simple but surprisingly accurate rendition of the annual mean carbon cycle for the global ocean. Nonetheless, OCMIP models are known to have seasonal biases which are typically attributed to their bulk parameterization of 'compensation depth'. Utilizing the criteria of surface Chl-a based attenuation of solar radiation and the minimum solar radiation required for production, we have proposed a new parameterization for a spatially and temporally varying 'compensation depth' which captures the seasonality in the production zone reasonably well. This new parameterization is shown to improve the seasonality of CO_2 fluxes, surface ocean pCO_2, biological export and new production in the major upwelling zones of the Indian Ocean. The seasonally varying compensation depth enriches the nutrient concentration in the upper ocean yielding more faithful biological exports which in turn leads to an accurate seasonality in the carbon cycle. The export production strengthens by $\sim 70\%$ over the western Arabian Sea during monsoon period and achieves a good balance between export and new production in the model. This underscores the importance of having a seasonal balance in model export and new productions for a better representation of the seasonality of carbon cycle over upwelling regions. The study also implies that both the biological and solubility pumps play an important role in the Indian Ocean upwelling zones.

Keywords: Indian Ocean upwelling zones, Carbon cycle, Seasonal cycle - CO_2 flux and Oceanic pCO_2, Biogeochemical model parameterization, Export production - New production balance, Solubility and Biological pump.

1. Introduction

The Indian Ocean is characterized by the unique seasonally reversing monsoon wind systems which act as the major physical drivers for the coastal and open ocean upwelling processes. The major upwelling systems in the Indian Ocean are (1) the western Arabian Sea (WAS; Ryther and Menzel, 1965; Smith et al., 2001; Sarma, 2004; Wiggert et al., 2005, 2006; Murtugudde et al., 2007; McCreary et al., 2009; Prasanna Kumar et al., 2010; Naqvi et al., 2010; Roxy et al., 2015) (2) the Sri Lanka Dome (SLD; Vinayachandran et al., 1998, 2004), (3) Java and Sumatra coasts (SC; Murtugudde et al., 1999a; Susanto et al., 2001; Osawa et al., 2010; Xing et al., 2012) and (4) the Seychelles-Chagos thermocline ridge (SCTR; Murtugudde et al., 1999b; Dilmahamod et al., 2016, Figure 1). The physical and biological processes and their variability over these key regions are inseparably tied to the strength of the monsoon winds and associated nutrient dynamics. The production and its variability over these coastal upwelling systems are a key concern for the fishing community, since they affect the day-to-day livelihood of the coastal populations (Harvell et al., 1999; Roxy et al., 2015; Praveen et al., 2016) and are important for the Indian Ocean rim countries due to their developing country status.

Arabian Sea is a highly productive coastal upwelling system characterized by phytoplankton blooms both in summer (Prasanna Kumar et al., 2001; Naqvi et al., 2003; Wiggert et al., 2005) and winter (Banse and McClain, 1986; Wiggert et al., 2000; Barber et al., 2001; Prasannakumar et al., 2001; Sarma, 2004). The Arabian Sea is known for the second largest Tuna fishing region in the Indian Ocean (Lee et al., 2005). The Somali and Omani upwelling regions experience phytoplankton blooms that are prominent with Net Primary Production (NPP) exceeding 435 g C m^{-2} yr^{-1} (Liao et al., 2016). On the other hand productivity over the SLD (Vinayachandran and Yamagata, 1998) is triggered by open ocean Ekman suction with strong Chl-a blooms during the

68 summer monsoon (Murtugudde et al., 1999a; Vinayachandran et al., 2004). Similarly, the SC

69 upwelling is basically due to the strong alongshore winds and its variation is associated with the

70 impact of equatorial and coastal Kelvin waves (Murtugudde et al., 2000, Valsala and Rao, 2016).

71 The interannual variability associated with the Java-Sumatra coastal upwelling is strongly

72 coupled with ENSO (ElNiño Southern Oscillation) through the Walker cell and Indonesian

73 throughflow (Susanto et al., 2001; Valsala et al., 2011) and peaks in July through August with a

74 potential new production of 0.1 Pg C yr^{-1} (Xing et al., 2012). The SCTR productivity has a large

75 spatial and interannual variability. The warmer upper ocean condition associated with El Niño

76 reduces the amplitude of subseasonal SST variability over the SCTR (Jung and Kirtman., 2016).

77 The Chl-a concentration peaks in summer when the southeast trade winds induce mixing and

78 initiate the upwelling of nutrient-rich water (Murtugudde et al., 1999a; Wiggert et al., 2006;

79 Vialard et al., 2009; Dilmahamod et al., 2016).

80 Understanding the biological production and variability in the upwelling systems is important

81 because it gives us crucial information regarding marine ecosystem variability (Colwell, 1996;

82 Harvell et al., 1999). The observations also provide vital insights into physical and biological

83 interactions of the ecosystem (Naqvi et al., 2010) as well as the biophysical feedbacks

84 (Murtugudde et al., 1999a), although limitations of sparse observations often force us to depend

85 on models to examine the large spatio-temporal variability of the ecosystem (Valsala et al.,

86 2013). Simple to intermediate complexity marine ecosystem models have been employed by

87 several of the previous studies (Sarmiento et al., 2000; Orr et al., 2001; Matsumoto et al., 2008).

88 However, the representation of marine ecosystem with proper parameterizations in models has

89 always been a daunting task. This is an impediment to the accurate representation of biological

90   primary and export productions in models (Friedrichs et al., 2006, 2007) and these issues also

91   impact the modeling of upper trophic levels (Lehodey et al., 2010).

92   Biological production can be quantified with a better understanding of primary production

93   which depends on water temperature, light and nutrient availability (Brock et al., 1993; Moisan

94   et al., 2002) and this became the key reason for parameterizing the production in models as one

95   or more combinations of these terms (Yamanaka et al., 2004). Any of these basic parameters can

96   be tweaked to alter production in models. For example, the availability of nutrients and light

97   determines the phytoplankton growth (Eppely et al., 1972) or growth rate (Boyd et al., 2013).

98   Stoichiometry and carbon-to-Chl-a ratios are other important factors to be considered in

99   modeling (Christian et al., 2001, Wang et al., 2009) but we will not consider them in this study.

100   The Ocean Carbon-cycle Model Intercomparison Project (OCMIP) greatly improved our

101   understanding of global carbon cycle (Najjar and Orr, 1998). OCMIP-II further introduced a

102   simple phosphate-dependent production term in biological models for long-term simulations of

103   the carbon cycle in response to anthropogenic climate change with an accurate annual mean state

104   (Najjar and Orr, 1998; Orr et al., 2001; Doney et al., 2004). However, the $OCMIP - II$ model

105   simulations come with a penalty of strong seasonal biases when compared with observations

106   (Orr et al., 2003). In this protocol, the community compensation depth (hereafter Zc) is defined

107   as the depth at which photosynthesis equals entire community respiration and the irradiance at

108   which this balance achieved is the compensation irradiance (E_{com}). Note that Zc is clearly

109   different from the conventional euphotic zone depth (Morel, 1988). Within Zc, the production of

110   organic phosphorous representing the biological production (in the present context the Net

111   Community Production; NCP) is given as $J_{prod} = \frac{1}{\tau}([PO_4] - [PO_4^*])$, where $[PO_4]$ is the model

112   phosphate concentration and $[PO_4^*]$ is observational phosphate concentration. τ is the restoration

113 timescale assumed to be 30 days. Whenever the model phosphate exceeds the observational

114 phosphate, it allows production. At Zc, the NCP is zero and above Zc the Net Primary

115 Production (NPP) exceeds the community respiration and the ecosystem will grow (Smetacek

116 and Passow, 1990; Gattuso et al., 2006; Sarmiento and Gruber, 2006; Regaudix-de-Gioux and

117 Duarte, 2010; Marra et al., 2014). However, Zc was held constant in time and space in OCMIP-II

118 models (Najjar and Orr, 1998; Matsumoto et al., 2008) because the OCMIP-II protocol takes a

119 minimalistic approach to biology and simplifies the model calculations with a very limited set of

120 state variables suitable for long term simulations when implemented in coarse resolution models

121 (Orr et al., 2005). However, in reality Zc varies in space and time (Najjar and Keeling, 1997) just

122 as the euphotic zone depth does as documented in ship measurements (Qasim, 1977, 1982). The

123 variation in Zc indicates the seasonality of the production zone itself.

124   Most of the biophysical models prescribe a constant value for Zc, e.g., a default value of

125 Zc = 75 m in OCMIP –II protocol (Najjar and Orr, 1998) and Zc = 100 m in Minnesota Earth

126 System Model (Matsumoto et al., 2008). Depending on the latitude, Zc varies between 50m and

127 100m in the real world (Najjar and Keeling, 1997). In our study we have attempted a novel

128 biological parameterization scheme for spatially and temporally varying Zc in the OCMIP–II

129 framework by representing the production as a function of solar radiation (Parsons et al., 1984)

130 and prescribed Chl-a. In this hypothesis, a spatially and temporally varying Zc is estimated from

131 the vertical attenuation of insolation by the surface Chl-a. The depth at which the insolation

132 reaches the compensation irradiance (chosen as 10 Wm^{-2}) is taken as Zc. Phosphorous is the

133 basic currency which limits the production within this varying Zc. This spatially and temporally

134 varying Zc represents the seasonality in the production zone which is lacking in the original

135 OCMIP-II protocol.

136   Regions of sustained upwelling like the eastern equatorial Pacific are well understood in

137   terms of the role of upwelling in increasing the surface water pCO_2 to drive an outgassing of CO_2

138   into the atmosphere (Feely et al., 2001; Valsala et al., 2014). The Indian Ocean on the other hand

139   experiences only seasonal upwelling which is relatively weak in the deep tropics but stronger off

140   the coasts of Somalia and Oman and in the SLD (Valsala et al., 2013). The relative importance of

141   the solubility vs. biological pump is not well understood. Our focus here on implementing

142   seasonality in Zc of OCMIP models nonetheless leads to new insights on the impact of improved

143   biological production on surface water pCO_2 and air-sea CO_2 fluxes. The improvements due to

144   the effect of a variable Zc over the Indian Ocean and the sensitivity experiments where

145   upwelling is muted strongly imply that the biological pump may play as much of a role as the

146   solubility pump in determining surface pCO_2 and CO_2 fluxes over the Indian Ocean.

147   The paper is organized as follows. Model, Data, and Methods are detailed in Section 2.

148   The spatially inhomogeneous Zc derived with the new parameterization and its impact on

149   simulated seasonality of biology and carbon cycle are detailed in Section 3. Further a conclusion

150   is provided in Section 4.

151

2. Model, Data, and Methods

2.1. Model

154   The study utilizes the Offline Ocean Tracer Transport Model (OTTM; Valsala et al., 2008)

155   coupled with OCMIP biogeochemistry model (Najjar and Orr, 1998). OTTM does not compute

156   currents and stratifications (i.e., temperature and salinity) on its own. It is capable of accepting

157   any ocean model or data-assimilated product as physical drivers. The physical drivers prescribed

158   include 4-dimensional currents (U, V, W), temperature, salinity, and 3-dimensional mixed layer

159   depth, surface freshwater and heat fluxes, surface wind stress and sea surface height. The

160   resolution of the model setup is similar to the parent model from which it borrows the physical

161   drivers. With the given input of Geophysical Fluid Dynamics Laboratory (GFDL) reanalysis data

162   (Chang et. al., 2012), the zonal and meridional resolutions are 1° with 360 grid points

163   longitudinally and 1° at higher latitudes but having a finer resolution of 0.8^o in the tropics, with

164   200 latitudinal grid points. The model has 50 vertical levels with 10m increment in the upper

165   225m and stretched vertical levels below 225m. The horizontal grids are formulated in spherical

166   coordinates and vertical grids are in z levels. The model employs a B-grid structure in which the

167   velocities are resolved at corners of the tracer grids. The model uses a centered-in-space and

168   centered-in-time (CSCT) numerical scheme along with an Asselin-Robert filter (Asselin, 1972)

169   to control the ripples in CSCT.

170   The tracer concentration (C) evolves with time as

171   $$\frac{\partial C}{\partial t} + U.\nabla_H C + W\frac{\partial C}{\partial z} = \frac{\partial}{\partial z}K_z\frac{\partial}{\partial z}C + \nabla_H.(K_h\nabla_H C) + J + F \qquad (1)$$

172   where ∇_H is the horizontal gradient operator, U and W are the horizontal and vertical velocities

173   respectively. K_z is the vertical mixing coefficient, and K_h is the two-dimensional diffusion

174   tensor. J represents any sink or source due to the internal consumption or production of the

175   tracer. F represents the emission or absorption of fluxes at the ocean surface. Here, the source

176   and sink terms are provided through the biogeochemical model. Vertical mixing is resolved in

177   the model using K- profile parameterization (KPP; Large et al., 1994).

178   In addition to KPP, the model uses a background vertical diffusion reported by Bryan and Lewis

179   (Bryan and Lewis, 1979). For horizontal mixing, model incorporates Redi fluxes (Redi, 1982)

180   and GM fluxes (Gent and Mcwilliams, 1990) which represent the eddy-induced variance in the

181   mean tracer transport. A weak Laplacian diffusion is also included in the model for

182   computational stability where the sharp gradient in concentration occurs.

2.2. Biogeochemical model

184   The biogeochemical model used in the study is based on the OCMIP – II protocol as

185   stated above. The main motivation of OCMIP–II protocol is to employ a minimalistic approach

186   to simulate the ocean carbon cycle with a nutrient restoration approach to calculate the oceanic

187   biological production (Najjar et al., 1992; Anderson and Sarmiento, 1995). The present version

188   of the model has four prognostic variables coupled with the circulation field, viz., inorganic

189   phosphorus (PO_4^{3-}), dissolved organic phosphorus (DOP), dissolved inorganic carbon (DIC) and

190   alkalinity (ALK). The basic currency for the biological model is phosphorous because of the

191   availability of a more extensive phosphate database and to eliminate the complexities associated

192   with nitrogen fixation and denitrification. Detailed model equations and variables are provided in

193   Appendix-A with only a brief description given below.

194   The production of organic phosphorus in the model using the nutrient restoring approach is given

195   by

196    $J_{prod} = \frac{1}{\tau}([PO_4] - [PO_4]^*)$ (2)

197                    $[PO_4] > [PO_4]^*$; Z < Zc

198    $J_{prod} = 0$ (3)

199                    $[PO_4] \leq [PO_4]^*$

200   Where J_{prod} represents the biogeochemical flows with respect to production of organic

201   phosphorous. $[PO_4]^*$ is the observed phosphate concentration and $\tau=30$ days is the restoration

202   time scale (Najjar et. al., 1992). The conversion of phosphorus to carbon is done by multiplying

203   Redfield ratio ($R_{C:P}= 117$).

204   The vertically integrated new production (g C m^{-2} yr^{-1}) in the model is defined as

$$New\ production = \int_{zc}^{0} -J_{prod}\ dz \qquad (4)$$

205   The export production (g C m^{-2} yr^{-1}) in the model is calculated as

$$Export\ production = (1 - \sigma) \int_{0}^{zc} J_{prod}\ dz \qquad (5)$$

206   Air-sea CO_2 flux in the model is estimated by,

207    $F = K_w\ \Delta\ pCO_2$ \qquad (6)

208   where K_w is gas transfer velocity and $\Delta\ pCO_2$ is the difference in partial pressure of carbon

209   dioxide between the ocean and atmosphere.

210   pCO$_2$ is calculated in the model by using DIC and ALK and is given by,

$$pCO_2 = \frac{[DIC]}{K_0} \frac{[H^+]^2}{[H^+]^2 + K_1[H^+] + K_1K_2} \qquad (7)$$

211   Where $[H^+]$ is calculated using Newton-Raphson iterative method (Press et. al., 1996, Najjar and

212   Orr, 1998). K_0 is the solubility constant of CO_2 and K_1, K_2 are the dissociation constant for

213   carbonic acid, respectively (Sarmiento and Gruber, 2006, Weiss, 1974, Mehrbach et al., 1973,

214   Dickson and Millero, 1987, Najjar and Orr, 1998).

215   Details of all parameters in the biogeochemical model and calculations of solubility and

216   biological pump are listed in Appendix-A. The design and validation of the physical model is

217   reported by Valsala et al., (2008, 2010b) and biogeochemical model by Najjar and Orr (1998).

218

2.3. Data

220   For validating the model results, observational datasets of CO_2 flux and pCO_2 are taken

221   from Takahashi et al., (2009). Satellite-derived NPP data were taken from Sea-viewing Wide

222   Field of view Sensor (SeaWiFS) Chl-a product, calculated using Vertically Generalized

223   Production Model (VGPM; Behrenfeld and Falkowski, 1997). The NPP data is scaled to export

224   production (EP) by multiplying with an e-ratio (e = 0.37) representative of Indian Ocean

225   upwelling zones (Sarmiento and Gruber, 2006, Laws et al., 2000; Falkowski et al., 2003). The

226   initial conditions for PO_4 are taken from the World Ocean Atlas (Garcia et al., 2014). Initial

227   conditions for DIC and ALK are taken from the Global Ocean Data Analysis Project (GLODAP;

228   Key et al., 2004) dataset. The dissolved Organic Phosphorous (DOP) is initialized with a

229   constant value of 0.02 μmol kg^{-1} (Najjar and Orr, 1998). The data sources and citations are

230   provided in the Acknowledgement.

231

2.4. Methods

233   A spin-up for 50 years from the given initial conditions is performed with the

234   climatological physical drivers. As the initial conditions are provided from a mean state of

235   observed climatology, this duration of spin-up is sufficient to reach statistical equilibrium in the

236   upper 1000 m (Le Quere et al., 2000). Atmospheric pCO_2 has been set to a value from the 1950s

237   in the spin-up run for calculating the air-sea CO_2 exchange. A seasonal cycle of atmospheric

238   pCO_2 has been prescribed as in Keeling et al. (1995).

239   After the spin-up, an interannual simulation for 50 years from 1961 to 2010 has been

240   carried out with the corresponding observed atmospheric pCO_2 described in Keeling et al.,

241   (1995). The first five years of the interannual run were looped five times through the physical

242   fields of 1961 repeatedly for a smooth merging of the spin-up restart to the interannual physical

243   variables. Since the study is focused on bias corrections to the seasonal cycle of pCO_2 and DIC

244   with a variable Zc, a model climatology for carbon cycle has been constructed from 1990 to

245   2010, which includes the anthropogenic increase of oceanic DIC in the climatological calculation

246   and is comparable with the Takahashi et al. (2009) observations.

247   Additional two sensitivity experiments have been performed separately by providing

248   annual mean currents or temperatures as drivers over selected regions of the basin in order to

249   segregate the role of varying Zc in improving the seasonality of carbon cycle. The aim of these

250   sensitivity experiments is to understand how successful the new parameterization for Zc is in

251   capturing the carbon cycle variability related to the upwelling episodes even though the seasonal

252   cycle in physics is suppressed. The model driven with annual mean currents suppresses the

253   effect of upwelling by muting the Ekman divergence over the region of interest. On the other

254   hand, the model forced with annual mean temperatures suppresses the cooling effect of

255   upwelling. A smoothing technique with linear interpolation ($U = U(1 - x) + \overline{U}x$) is applied to

256   the offline-data in order to blend the annual mean fields ($\overline{U}$) provided to the selected region with

257   the rest of the domain (U) in order to reduce a sudden transition at the boundaries. Here x

258   represents an index which varies between 0 and 1 within a distance of 10^0 from the boundaries of

259   the region of interest to the rest of the model domain. Results of sensitivity experiments are

260   provided in supplementary material.

261

2.5. Community compensation depth (Zc) parameterization

263   The OCMIP – II protocol separates the production and consumption zones by a depth termed

264   as compensation depth (Zc); the depth at which photosynthesis is large enough to balance the

265   community respiration (i.e., both the autotrophic and heterotrophic respiration). At the

266   community compensation depth, the NCP is zero i.e., $NCP = NPP - R_h = 0$, (i.e., $NPP = GPP -$

267   R_a), GPP is gross primary production, and R_h and Ra are the heterotrophic and autotrophic

268   respirations, respectively (Smetacek and Passow, 1990; Najjar and Orr, 1998; Gattuso et al.,

269   2006; Regaudix-de-Gioux and Duarte, 2010; Marra et al., 2014). The light intensity at Zc is

270   compensation irradiance (E_{com}), the irradiance at which the gross community primary production

271   balances respiratory carbon losses for the entire community (Gattuso et al., 2006; Regaudix-de-

272   Gioux and Duarte, 2010). We define a spatially and temporally varying compensation depth

273   (hereafter varZc) as a depth where compensation irradiance (attenuated by surface Chl-a, Jerlov

274   et al., 1976) reaches a minimum value of 10 W m^{-2}. In this way, the varZc has both spatio-

275   temporal variability of light as well as Chl-a. The Chl-a is given as monthly climatology as

276   constructed from satellite data. Observations show that the primary production reduces rapidly to

277   20% or less of the surface value below a threshold of 10 W m^{-2} (Parsons et al., 1984; Ryther,

278   1956; Sarmiento and Gruber, 2006). Moreover higher ocean temperatures (those in the tropics)

279   enhance the respiration rates resulting in high compensation irradiance (Parsons et al., 1984;

280   Ryther, 1956; Lopez-Urrutia et al., 2006; Regaudix-de-Gioux and Duarte, 2010). A study by

281 Regaudix-de-Gioux and Duarte (2010) reported the mean value of compensation irradiance over

282 the Arabian Sea as 0.4 ± 0.2 mol photon m^{-2} day^{-1} which is close to 10 W m^{-2} day^{-1}.

283   Figure 2 compares the scatter of average relative photosynthesis (See Appendix-B for

284 details) within varZc as a function of solar radiation for the Indian Ocean. This encapsulates the

285 corresponding curve from the observations for the major phytoplankton species in the ocean such

286 as diatoms, green algae and dinoflagellates (Ryther et al., 1956; Parsons et al., 1984; Sarmiento

287 and Gruber, 2006). The model permits 100% production of organic phosphorus for radiation

288 above 10 W m^{-2}. However the availability of phosphate concentration in the model acts as an

289 additional limit for production which indirectly represents the photoinhibition at higher

290 irradiance; for example, in the oligotrophic gyres.

291

292 3. **Results and Discussions**

293   The inclusion of seasonality in Zc by way of parameterizing varZc leads to a remarkable

294 spatio-temporal variability in Zc (Figure 3). Zc over the Arabian Sea varies from 10 m to 25 m

295 during December to February (DJF) and deepens down to 45 m during March to May (MAM)

296 due to the increase in the surface solar radiation. During the monsoon season i.e., June to

297 September (JJAS), Zc again shoals to 10 m - 35 m due to the attenuation of solar radiation by the

298 increased biological production (Chl-a). During October to November (ON), Zc slightly deepens

299 as compared to JJAS.

300 The Bay of Bengal Zc deepens from 35 m to 40 m during DJF and further deepens to 50 m

301 during MAM when the solar radiation is maximum and biological production is minimum

302 (Prasannakumar et al., 2002). Further reduction of Zc can be seen through JJAS as a result of a

303 reduction in solar radiation during monsoon cloud cover. Zc during ON is 35 m on average.

304 The equatorial Indian Ocean can be seen as a belt of 40 m - 45 m Zc throughout the season

305 except for JJAS. During JJAS, a shallow Zc is seen near the coastal Arabian Sea (around 10 m to

306 35 m) presumably due to the coastal Chl-a blooms. Deep Zc off the coast of Sumatra ($\sim$ 40 m to

307 50 m) is found during JJAS. Java-Sumatra coastal upwelling is centered on SON (Susanto et al.,

308 2001) and upwelling originates at around 100 m depth (Valsala and Maksyutov, 2010a; Xing et

309 al., 2012).

310 Southward of 10^oS in the oligotrophic gyre region, Zc varies from 40 m to more than 60 m

311 throughout the year. A conspicuous feature observed while parameterizing the solar radiation

312 and Chl-a dependent Zc is that its maximum value never crosses 75 m especially in the Indian

313 Ocean which is the value specified in OCMIP-II models. The cutoff depth of 75 m in OCMIP-II

314 is obtained from observing the seasonal variance in oxygen data (Najjar and Keeling, 1997) as an

315 indicator of the production zone. However, our results show that parameterizing a production

316 zone based on solar radiation and Chl-a predicts a production zone and its variability that is

317 largely less than 75 m. The relevance of varZc in the seasonality of the modeled carbon cycle is

318 illustrated as follows.

319

320 **3.1. Simulated seasonal cycle of pCO$_2$ and CO$_2$ fluxes**

321   The annual mean biases in simulated CO$_2$ fluxes and pCO$_2$ were evaluated by comparing

322 with Takahashi et al., (2009) observations (Figure 4). The model biases are significantly reduced

323   with the implementation of varZc compared to that of the constant Zc (hereinafter constZc). A

324   notable reduction in pCO_2 bias (by $\sim$ 10µatm) is observed along the WAS (Figure 4d).

325   In order to address the role of the new biological parameterization of a variable Zc, we

326   zoom in on four key regions where the biological production and CO_2 fluxes are prominent in the

327   Indian Ocean with additional sensitivity experiments (see Introduction and references therein).

328   The regions (boxes shown in Figure 1) we considered are, (1) Western Arabian Sea (WAS;

329    $40^oE:65^oE$, $5^oS:25^oN$) (2) Sri Lanka Dome (SLD; $81^oE:90^oE$, $0^o:10^oN$) and (3) Sumatra Coast

330   (SC; $90^oE:110^oE$, $0^o:10^oS$) (4) Seychelles-Chagos Thermocline Ridge (SCTR; $50^oE:80^oE$,

331    $5^oS:10^oS$; Figure 1). The seasonal variations of Zc over these selected key regions are shown in

332   Figure 5. A detailed analysis of CO_2 fluxes, pCO_2, biological export and new productions and the

333   impact of varZc simulations in improving the strength of biological pump and solubility pump

334   for these key regions are presented below.

335

336   **3.2. Western Arabian Sea (WAS)**

337   The WAS Zc has a double peak pattern over the annual cycle. During the February-March

338   period, Zc deepens down to a maximum of 43.85 ± 2.3 m into March and then shoals to 25.75 ±

339   1.5 m (Figure 5) during the monsoon period (uncertainty represents the interannual standard

340   deviations of monthly data from 1990-2010). This shoaling of Zc depth during the monsoon

341   indicates the potential ability of the present biological parameterization to capture the wind-

342   driven upwelling related production in the WAS. During the post-monsoon period, the second

343   deepening of Zc occurs during November with a maximum depth of 34.91 ± 2.2 m. The ability to

344   represent the seasonality of the production zone renders a unique improvement in CO_2 flux

345   variability especially in the WAS in comparison to the OCMIP-II experiments (Orr et al, 2003;

346   Figure 6a).

347   OCMIP –II simulations with a constZc of 75 m underestimate the CO_2 flux when compared

348   to the observations of Takahashi et al. (2009). This underestimation is clearly visible during the

349   monsoon period. Our simulations with the varZc result in a better seasonality of CO_2 flux when

350   compared with Takahashi et al. (2009) observations (Figure 6a). The improvement due to the

351   varZc scheme is able to represent the seasonality of CO_2 flux better especially during the

352   monsoon period when wind-driven upwelling is dominant. Obviously, the relative role of the

353   biological and solubility pumps have to be deciphered in this context.

354   The CO_2 flux during July from observations, constZc, and varZc simulations are 3.09 mol m^{-2}

355   yr^{-1}, 1.82 ± 0.4 mol m^{-2} yr^{-1} and 3.10 ± 0.5 mol m^{-2} yr^{-1}, respectively. Southwesterly wind-driven

356   upwelling over the WAS especially off the Somali coast (Smith and Codispoti, 1980; Schott,

357   1983; Smith, 1984) and Oman (Bruce, 1974; Smith and Bottero, 1977; Swallow, 1984; Bauer et

358   al., 1991), pulls nutrient-rich subsurface waters closer to the surface while the available turbulent

359   energy due to the strong winds lead to mixed layer entrainment of the nutrients resulting in a

360   strong surface phytoplankton bloom (Krey and Babenerd, 1976; Banse, 1987; Bauer, 1991;

361   Brock et al, 1991). This regional bloom extends over 700 km offshore from the Omani coast due

362   to upward Ekman pumping driven by strong, positive wind-stress curl to the northwest of the low

363   level jet axis and the offshore advection (Bauer et al., 1991; Brock et al., 1991; Brock and

364   McClain, 1992a, b; Murtugudde and Busalacchi, 1999, Valsala, 2009) resulting in strong

365   outgassing of CO_2 flux and an enhanced pCO_2 in the WAS (Valsala and Maksyutov, 2013;

366   Sarma et al., 2002). The seasonal mean CO_2 flux during the southwest monsoon period (JJAS)

367   for constZc and varZc simulations are 1.44 ± 0.2 mol m^{-2} yr^{-1} and 2.31 ± 0.4 mol m^{-2} yr^{-1},

368   respectively. The biological parameterization of varZc considerably improves the average CO_2

369   flux during the monsoon period by 0.86 ± 0.1 mol m^{-2} yr^{-1}. The annual mean CO_2 flux from

370   observations, constZc and varZc simulations are 0.94 mol m^{-2} yr^{-1}, 0.80 ± 0.17 mol m^{-2} yr^{-1} and

371   1.07 ± 0.2 mol m^{-2} yr^{-1}, respectively. The annual mean CO_2 flux is improved by 0.27 ± 0.05 mol

372   m^{-2} yr^{-1}.

373   Seasonality in pCO_2 also shows a remarkable improvement during the southwest monsoon

374   period (Figure 6b). The pCO_2 with constZc is considerably lower at a value of 385.22 ± 3.5 µatm

375   during June compared to observational values of 392.83 µatm. However, varZc simulation

376   performs better in terms of pCO_2 variability. The peak value of pCO_2 reaches up to 405.42 ± 5.8

377   µatm. The seasonal mean pCO_2 during the Southwest monsoon period from observations,

378   constZc, and varZc simulations are 397.58 µatm, 389.18 ± 3.6 µatm and 399.95 ± 5.0 µatm,

379   respectively. The improvement in pCO_2 by varZc simulation is 10.76 ± 1.3 µatm when compared

380   with the constZc simulation. This clearly shows that constZc simulation fails to capture the pCO_2

381   driven by upwelling during the Southwest monsoon while the varZc simulation is demonstrably

382   better in representing this seasonal increase. The annual mean pCO_2 from observations, constZc,

383   and varZc simulations are 394.69 µatm, 389.62 ± 3.9 µatm and 391.19 ± 4.7 µatm, respectively.

384   However, it is worth mentioning that there are parts of the year where the constZc performs

385   better compared to varZc. For instance, during MAM as well as in November, the constZc

386   simulation yields a better comparison with the observed pCO_2 whereas varZc simulation yields a

387   reduced magnitude of pCO_2. This may well indicate the biological vs. solubility pump controls

388   on pCO_2 during the intermonsoons. The role of mesoscale variability in the ocean dynamics may

389   also play a role (Valsala and Murtugudde, 2015). Nevertheless, during the most important season

390 (JJAS) when the pCO_2, CO_2 fluxes, and biological production are found to be dominant in the

391 Arabian Sea, the varZc produces a better simulation.

392   The improvements shown by the use of varZc in the simulation of CO_2 flux and pCO_2 can be

393 elicited by further analysis of the model biological production. Figure 7 shows the comparison of

394 model export production and new production with observational export production from

395 satellite-derived NPP for constZc and varZc simulations. The model export production in the

396 constZc simulation is much weaker when compared to varZc simulation. The varZc simulation

397 has improved the model export production. Theoretically, the new and export productions in the

398 model should be in balance with each other (Eppley and Peterson, 1979). The constZc export

399 production is much weaker than new production and it is not in balance. In contrast, the varZc

400 simulation yields a close balance among them.

401   Compared with the observational export production which peaks in August at a value of

402 154.78 g C m^{-2} yr^{-1}, the varZc simulated export and new productions peak at a value of 160.44 ±

403 20.4 g C m^{-2} yr^{-1} and 167.18 ± 24.0 g C m^{-2} yr^{-1}, respectively, but in July. A similar peak can be

404 observed in constZc simulated new production as well, with a value of 178.19 ± 28.0 g C m^{-2} yr^{-}

405 ^{1}. This apparent shift of one month during JJAS in the model export production as well as in the

406 new production is noted as a caveat in the present set up which will need further investigation.

407 Arabian Sea production is not just limited by nutrients but also the dust inputs (Wiggert et al.,

408 2006). The dust-induced primary production in the WAS, especially over the Oman coast is

409 noted during August (Liao et al., 2016). The mesoscale variability in the circulation and its

410 impact on production and carbon cycle are also a limiting factor in this model as noted above.

411   The seasonal mean export production during the southwest monsoon period from satellite-

412   derived estimate is 123.57 g C m^{-2} yr^{-1}, whereas for constZc and varZc simulations it is 84.81 ±

413   16.0 g C m^{-2} yr^{-1} and 147.19 ± 23.8 g C m^{-2} yr^{-1}, respectively. The new biological

414   parameterization strengthens the model export production by 62.38 ± 7.8 g C m^{-2} yr^{-1} for the

415   southwest monsoon period, which is over a 70% increase. This indicates a considerable impact

416   of the biological pump in the model simulated CO_2 flux and pCO_2 over the WAS. For constZc

417   simulation, the computed new production is slightly higher (150.84 ± 27.9 g C m^{-2} yr^{-1}) than that

418   of varZc (133.03 ± 19.5 g C m^{-2} yr^{-1}). The annual mean export production from observations,

419   constZc and varZc simulations are 94.31 g C m^{-2} yr^{-1}, 77.41 ± 15.1 g C m^{-2} yr^{-1} and 122.54 ± 25.2

420   g C m^{-2} yr^{-1}, respectively.

421   To understand how the varZc parameterization strengthens the export production in the

422   model, we have analyzed the phosphate profiles. It appears that the varZc parameterization

423   allows more phosphate concentration (Figure 8a, b) in the production zone and thereby increases

424   the corresponding biological production (Figure 8c, d). The net export production in the model

425   during JJAS is consistent with the satellite data (Figure 7b). However, in the constZc case, the

426   exports are rather 'flat' throughout the season with a poor representation of seasonal biological

427   export. The Table 1-4 summarize all the values discussed here.

428   The impact of varZc in the biological and solubility pumps is computed as per Louanchi et

429   al., (1996, see Appendix A). The varZc parameterization strengthens the biological as well as the

430   solubility pump in the model thereby modifying the phosphate profiles and achieves a seasonal

431   balance in export versus new production (Figure 9a). During the monsoon period, the varZc

432   simulation increases the strength of the solubility and biological pumps by 10.43 ± 1.3 g C m^{-2}

433   yr^{-1} and 106.52 ± 9 g C m^{-2} yr^{-1}, respectively (see Table 5 and 6). Similarly, the annual mean

434 strength of solubility pump and the biological pump are increased by 3.29 ± 0.6 g C m^{-2} yr^{-1} and

435 81.18 ± 9.92 g C m^{-2} yr^{-1}, respectively. This supports the fact that the varZc parameterization

436 basically modifies the biological and solubility pumps in the model simulation and thereby

437 improves the seasonal cycle of CO_2 flux and pCO_2.

438

3.3 Sri Lanka Dome (SLD)

440   The seasonal variation in Zc for SLD has a similar pattern as that of WAS. Zc deepens to its

441 maximum during March up to 45.23 ± 0.3 m and reaches its minimum during the following

442 monsoon period at 30.79 ± 1.5 m (Figure 5). The similarities of varZc between WAS and SLD

443 indicates that they both are under similar cycles of solar influx and biological production. The

444 SLD Chl-a dominates only up to July (Vinayachandran et al., 2004) which explains why

445 production with varZc increases earlier compared to WAS which occurs during ASO.

446   The seasonality in CO_2 flux and pCO_2 were compared with Takahashi et al., (2009)

447 observations (Figure 10). varZc results in a slight improvement in CO_2 flux when compared with

448 constZc (Figure 10a). However, both constZc and varZc simulations underestimate the

449 magnitude of CO_2 flux when compared with observations. The seasonal mean CO_2 flux during

450 the monsoon period is 1.79 mol m^{-2} yr^{-1} from observations, which means SLD region is a source

451 of CO_2. But the mean values of constZc and varZc simulations yield flux values of -0.008 ± 0.2

452 mol m^{-2} yr^{-1} and 0.24 ± 0.2 mol m^{-2} yr^{-1}, respectively. The constZc simulation misrepresents the

453 SLD region as a sink of CO_2 during monsoon period which is opposite to that of observations.

454 The varZc simulation corrects this misrepresentation to a source albeit at a smaller magnitude by

455   0.24 ± 0.09 mol m^{-2} yr^{-1} for the monsoon period. Compared to observations, the varZc case

456   underestimates the magnitude of JJAS mean by 1.55 mol m^{-2} yr^{-1}.

457   The annual mean CO_2 fluxes for constZc and varZc simulations are -0.02 ± 0.1 mol m^{-2} yr^{-1}

458   and 0.10 ± 0.2 mol m^{-2} yr^{-1}, respectively. The varZc parameterization leads to an improvement of

459   0.13 ± 0.1 mol m^{-2} yr^{-1} in the annual mean CO_2 flux when compared with constZc simulation.

460   The observational annual mean of CO_2 flux is 0.80 mol m^{-2} yr^{-1} which is highly underestimated

461   by both simulations. This indicates a regulation of biological production of the region by varZc

462   which makes this region a source of CO_2 during monsoon. The role of the solubility pump may

463   also be underestimated due to the biases in the physical drivers and the lack of mesoscale eddy

464   activities in these simulations (Prasanna Kumar et al., 2002; Valsala and Murtugudde, 2015).

465   The seasonality of pCO_2 (Figure 10b) especially in the monsoon period is significantly

466   improved. The mean pCO_2 during the monsoon season from observation over the SLD region is

467   382.44 µatm. The seasonal mean pCO_2 during monsoon period for constZc and varZc

468   simulations are 371.67 ± 6.04 µatm and 379.24 ± 8.9 µatm, respectively. The annual mean pCO_2

469   from observations, constZc, and varZc simulations are 380.21 µatm, 370.76 ± 6.1 µatm and

470   374.94 ± 9.6 µatm, respectively. varZc simulations improve the JJAS mean pCO_2 by 7.56 ± 2.8

471   µatm and the annual mean pCO_2 by 4.18 ± 3.5 µatm, which is reflected in CO_2 flux as well. This

472   is likely due to the impact of new biological parameterization in capturing the episodic upwelling

473   in the SLD region which is further investigated by looking at its biological production.

474   The SLD biological production is highly exaggerated by the model for both constZc and

475   varZc simulations (Figure 11a, b). The seasonal mean biological export for the monsoon period

476   is 51.54 g C m^{-2} yr^{-1} as per satellite-derived estimates. However, the constZc and varZc

477 simulations overestimate it at 167.71 ± 59.04 g C m^{-2} yr^{-1} and 151.51 ± 46.4 g C m^{-2} yr^{-1},

478 respectively. This exaggerated export is visible in climatological annual means where for

479 constZc and varZc simulations they are 144.43 ± 49.8 g C m^{-2} yr^{-1} and 156.08 ± 43.8 g C m^{-2} yr^{-1},

480 respectively.

481 For constZc simulation, new production is overestimated from March to October when

482 compared to observations and the second peak is observed in November (Figure 11a). But the

483 overestimate in new production with varZc is observed only during JJAS period by an amount of

484 26.23 g C m^{-2} yr^{-1}. For the SLD region, the varZc parameterization overestimates the export

485 production but minimizes the excess new production, especially in the monsoon period by 64.15

486 ± 36.4 g C m^{-2} yr^{-1}. This indicates that the varZc parameterization is somewhat successful in

487 capturing the upwelling episode during the monsoon over SLD. All values are summarized in

488 Tables 1 to 4.

489 The solubility and biological pumps are modified by the varZc parameterization significantly

490 when compared with the constZc simulation (Figure 9b). Over the monsoon period, the strength

491 of the solubility and biological pumps are improved by 2.81 ± 1.1 g C m^{-2} yr^{-1} and 66.68 ± 9.7 g

492 C m^{-2} yr^{-1}, respectively. Similarly, the annual mean strength of solubility and biological pump

493 are increased by 0.99 ± 1.2 g C m^{-2} yr^{-1} and 52.5 ± 5.1 g C m^{-2} yr^{-1} respectively. All values are

494 provided in Table 5 and 6.

495

496 **3.4 Sumatra Coast (SC)**

497 The seasonal variation in Zc over the SC region lies between 40 m and 46 m (Figure 5). The

498 seasonal maximum occurs during JFM, especially in March with a depth of 45.5 m. During the

499 monsoon period, Zc shoals slightly with a minimum of 41.1 m in July. The variation in Zc is

500 relatively small as compared to the other regions which is consistent with its relatively low

501 production throughout the year.

502 The seasonality of CO_2 flux and pCO_2 captured by constZc and varZc simulations are shown

503 in Figure 12a, b. The varZc simulations overestimate both CO_2 flux and pCO_2, especially during

504 the monsoon. It is found that the constZc simulation is better compared to varZc simulation. The

505 varZc simulation overestimates the seasonal mean CO_2 flux and pCO_2 by 1.19 mol m^{-2} yr^{-1} and

506 29.61 μatm, respectively, compared to observations (Table 1). However, constZc produces a

507 better estimate compared with observations for CO_2 flux and pCO_2. The constZc simulation also

508 delivers a better annual mean than varZc (Table 1, 2). The annual mean bias in constZc and

509 varZc simulations for CO_2 flux is -0.0033 mol m^{-2} yr^{-1} and 0.31 mol m^{-2} yr^{-1}, respectively.

510 Similarly, pCO_2 bias is 1.95 μatm and 9.07 μatm for constZc and varZc simulations.

511 Biological production simulated by the model along SC explains the overestimation of CO_2

512 flux and pCO_2 (Figure 13). Both constZc and varZc simulations greatly overestimate export

513 production in the model. However, a small enhancement in the new production during JJAS in

514 constZc case is an indicator of upwelling episodes. The seasonal mean new production during

515 the monsoon from constZc and varZc are 63.64 ± 30.9 g C m^{-2} yr^{-1} and 78.11 ± 29.1 g C m^{-2} yr^{-1},

516 respectively (Table 4). The seasonal mean export production during the monsoon from

517 observations is 58.87 g C m^{-2} yr^{-1} (Table 3). The constZc simulation represents a better new

518 production, which is seen as a relatively small exaggeration of CO_2 flux and pCO_2. The

519 biological response of SC is found to be better with constZc which is in contradiction to a

520 general improvement found with varZc in the other regions examined here. Such discrepancies

521 over the SC could be due to the effect of Indonesian Throughflow (Bates et al., 2006) which is

522   not completely resolved in the model due to coarse spatial resolution (also see Valsala and

523   Maksyutov, 2010a).

524   The overestimation of export production by varZc simulation is also evident by the increase

525   in strength of the biological and solubility pumps, respectively (Figure 9c). The annual mean and

526   JJAS mean DIC increases in the production zone due to the biological pump are 67.21 ± 1.3 g C

527   m^{-2} yr^{-1} and 83.62 ± 0.5 g C m^{-2} yr^{-1}, respectively. Similarly the increase in DIC due to the effect

528   of solubility pump during the JJAS period and annual mean are 10.95 ± 5.2 g C m^{-2} yr^{-1} and 3.87

529   ± 2.2 g C m^{-2} yr^{-1} respectively (see table 5 and 6).

530

531   **3.5 Seychelles-Chagos Thermocline Ridge (SCTR)**

532   The SCTR is a unique open-ocean upwelling region with a prominent variability in air-sea

533   interactions (Xie et al., 2002). Wind-driven mixing and upwelling of subsurface nutrient-rich

534   water play a major role in the biological production of this region (Dilmahamod et al., 2016).

535   The seasonal cycle in Zc is shown in Figure 5. The maximum Zc occurs in November at about

536   44.94 m and the minimum at 33.2 m in July. The shoaling of Zc during the monsoon period

537   shows that the biological parameterization captures the response to upwelling over this region.

538   The seasonality of CO_2 flux and pCO_2 are shown in Figure 14. The Takahashi observations

539   of CO_2 flux show a peak in June with outgassing of CO_2 during the upwelling episodes.

540   However, both constZc and varZc simulations underestimate this variability. The seasonality of

541   CO_2 flux in varZc shows a significant improvement when compared to constZc simulation, but

542   underestimated when compared to observations. The seasonal mean CO_2 flux during the

543   monsoon from observations, constZc and varZc simulations are 0.82 mol m^{-2} yr^{-1}, -0.32 ± 0.3

544 mol m^{-2} yr^{-1} and -0.05 ± 0.4 mol m^{-2} yr^{-1}, respectively. This represents a reduction in the seasonal

545 mean sink of CO_2 flux in the SCTR region during the monsoon by 0.27 ± 0.1 mol m^{-2} yr^{-1}

546 bringing it closer to a source region (see Table 1 for details).

547 The improved CO_2 flux is also supported by the seasonal cycle in pCO_2. Based on

548 observations, the seasonal mean of pCO_2 with constZc during JJAS is underestimated by 11.47

549 µatm, varZc simulation underestimates it by 6.45 µatm. So it is evident that varZc simulation

550 capture the upwelling episodes better, marked by a larger pCO_2 during JJAS period. However,

551 the magnitude of pCO_2 is still underestimated compared to observations (Table 2).

552 Figure 15 shows the biological production of constZc and varZc simulations for SCTR. It is

553 clear that both simulations overestimate the export production and underestimate the new

554 production. The JJAS mean export production from observations, constZc and varZc are 51.08 g

555 C m^{-2} yr^{-1}, 57.39 ± 14.2 g C m^{-2} yr^{-1} and 99.23 ± 29.8 g C m^{-2} yr^{-1}, respectively. The varZc

556 simulations exaggerate the model export production by 48.14 g C m^{-2} yr^{-1}. The varZc simulation

557 improves the JJAS mean new production by 1.14 ± 2.2 g C m^{-2} yr^{-1} (Table 4). The DIC variations

558 due to the biological pump over the monsoon period and the annual mean also correspond to the

559 exaggerated export production. During the monsoon period, the varZc simulation strengthens the

560 biological and solubility pumps by 72.64 ± 6.2 g C m^{-2} yr^{-1} and -4.56 ± 1.6 g C m^{-2} yr^{-1},

561 respectively, when compared to the constZc simulation (Figure 9d). This is also reflected in the

562 annual mean DIC variations due to the biological and solubility pump effects (see table 5 and 6).

563 This slight improvement in the model new production, especially during the monsoon period

564 signals that the varZc better captures the upwelling over SCTR. Considering the annual mean

565 values of model export and new production, constZc simulation is reasonably faithful to

566 observations.

567   The underestimation of CO_2 and pCO_2, as well as the exaggeration of model export

568   production and a slight, overestimate in model new production may be due to two reasons; (1)

569   SCTR is a strongly coupled region with remote forcing of the mixed layer − thermocline

570   interactions (Zhou et al., 2008) which can affect the seasonality in biological production that the

571   model may not be resolving reasonably, (2) the bias associated with physical drivers, especially

572   wind stress may underestimate the CO_2 flux as well biological production. A similar

573   overestimation of biological production was also reported in a coupled biophysical model

574   (Dilmahamod et al., 2016).

575   Table 1 − 4 shows the entire summary of seasonal and annual mean CO_2 flux, pCO_2 and

576   biological production reported in Section 3.

577

4. Summary and Conclusions

579   A spatially and temporally varying Zc parameterization as a function of solar radiation and

580   Chl-a is implemented in the biological pump model of OCMIP-II for a detailed analysis of

581   biological fluxes in the upwelling zones of the Indian Ocean. The varZc parameterization

582   improves the seasonality of model CO_2 flux and pCO_2 variability, especially during the monsoon

583   period. A significant improvement is observed in WAS where the monsoon wind-driven

584   upwelling dominates biological production. The magnitude of CO_2 flux matches with

585   observations, especially in July when monsoon winds are at their peak. Monsoon triggers

586   upwelling in SLD as well which acts as a source of CO_2 to the atmosphere. The seasonal and

587   annual mean are underestimated with constZc and the SLD is reduced to a sink of CO_2 flux. The

588   varZc simulation modifies the seasonal and annual means of the CO_2 flux of SLD and depict it as

589 a source of CO_2 especially during the monsoon, but the magnitude is still underestimated

590 compared to Takahashi et al. (2009) observations. The SCTR variability is underestimated by

591 both constZc and varZc simulations, portraying it as a CO_2 sink region whereas observations

592 over the monsoon period indicate that the thermocline ridge driven by the open ocean wind-

593 stress curl is, in fact, an oceanic source of CO_2. However, the varZc simulation reduces the

594 magnitude of the sink in this region bringing it relatively close to observations.

595 VarZc biological parameterization strengthens the export and new productions in the model,

596 which allows it to represent a better seasonal cycle of CO_2 flux and pCO_2 over the study regions.

597 The WAS export production is remarkably improved by 62.37 ± 7.8 g C m^{-2} yr^{-1} compared to

598 constZc. This supports our conclusion that the varZc parameterization increases the strength of

599 biological export in the model. Over the SLD, the JJAS seasonal mean export and new

600 production are underestimated in varZc compared to constZc simulations, but the annual mean

601 export production is improved. Export production at SC and SCTR are highly exaggerated and

602 there is hardly any improvement in new production with a variable Zc especially over the

603 monsoon period. The inability of varZc parameterization to improve the seasonality of SC and

604 SCTR may be due to the interannual variability of biological production associated with the

605 Indonesian throughflow and remote forcing of the mixed layer-thermocline interactions and the

606 effect of biases in the wind stress data used as a physical driver in the model.

607 Sensitivity experiments carried out by prescribing annual mean currents or temperatures over

608 selected subdomains reveal that the varZc retains the seasonality of carbon fluxes, pCO_2, and

609 export and new productions closer to observations. This strongly supports our contention that

610 varZc parameterization improves export and new productions and it is also efficient in capturing

611 upwelling episodes of the study regions. This points out the significant role of having a close

612   balance in seasonal biological export and new production in models to capture the seasonality in

613   the carbon cycle. This also confirms the role of biological and solubility pumps in producing the

614   seasonality of carbon cycle in the upwelling zones.

615   However, the underestimation of the seasonality of CO_2 flux over the SLD and

616   overestimation over the SC as well as the SCTR are a cautionary flag for the study. This

617   uncertainty poses an important scientific question as to whether the model biology over the SC

618   and SCTR region is not resolving the seasonality in CO_2 flux and pCO_2 properly or whether the

619   seasonality in the Zc is not able to fully capture the biological processes.

620   To address these questions we have used an inverse modeling approach (Bayesian inversion)

621   in order to optimize the spatially and temporally varying Zc using surface pCO_2 as the

622   observational constraint and computed the optimized biological production. The results will be

623   reported elsewhere.

624

625

626

627

628

629

630

631

632 **Appendix – A**

633 The time evolution equations of the model variables are given by

$$\frac{d[PO_4]}{dt} = L([PO_4]) + J_{PO_4} \qquad (A1)$$

$$\frac{d[DOP]}{dt} = L([DOP]) + J_{DOP} \qquad (A2)$$

$$\frac{dDIC}{dt} = L([DIC]) + J_{DIC} + J_g DIC + J_v DIC \qquad (A3)$$

$$\frac{d[ALK]}{dt} = L([ALK]) + J_{ALK} + J_v ALK \qquad (A4)$$

634 Where L is the 3D transport operator, which represents the effects of advection, diffusion, and

635 convection. [ ] or square brackets indicate the concentrations in mol m^{-3}. $J_{PO_4}, J_{DOP}, J_{DIC}, J_{ALK}$

636 are the biological source/sink terms and $J_v DIC$, $J_v ALK$ are the virtual source-sink terms

637 representing the changes in surface DIC and ALK, respectively, due to evaporation and

638 precipitation. $J_g DIC$ is the source-sink term due to air-sea exchange of CO_2.

639 The following equations represent for the biological processes in the model

640 For $Z < Zc$,

641 $J_{prod} = \frac{1}{\tau}([PO_4] - [PO_4^*]), \qquad [PO_4] > [PO_4^*]$ (A5)

642 $J_{DOP} = \sigma J_{prod} - \kappa[DOP]$ (A6)

643 $J_{PO4} = -J_{prod} + \kappa[DOP]$ (A7)

644     $J_{ca} = Rr_{C:P}(1 - \sigma)J_{prod}$ (A8)

645     $J_{DIC} = r_{C:P}J_{PO4} + J_{ca}$ (A9)

646     $J_{ALK} = -r_{N:P}J_{PO4} + 2J_{ca}$ (A10)

647   For Z >Zc,

648     $J_{prod} = 0,$ $[PO_4] \leq [PO_4^*]$ (A11)

649     $J_{DOP} = -\kappa[DOP]$ (A12)

650     $J_{PO4} = -\frac{\partial F}{\partial Z} + \kappa[DOP]$ (A13)

651     $F_c = (1 - \sigma)\int_0^{Zc} J_{prod}\, dZ$ (A14)

652     $F(Z) = F_c\left(\frac{Z}{Zc}\right)^{-a}$ (A15)

653     $J_{ca} = -\frac{\partial F_{Ca}}{\partial Z}$ (A16)

654     $F_{Ca} = Rr_{C:P}F_C e^{-(Z-Zc)/d}$ (A17)

655   Where Z is the depth and Zc is the compensation depth in the model. J_{prod} , J_{Ca} represents the

656   biogeochemical flows with respect to production and calcification. Within Zc, the production of

657   organic phosphorous in the model J_{prod} is calculated using equation A5. $[PO_4]$ is the model

658   phosphate concentration and $[PO_4^*]$ is observational phosphate. τ is the restoration timescale

659   assumed to be 30 days. Whenever the model phosphate exceeds the observational phosphate, it

660   allows production, below which the production is zero. The observational phosphate data were

661   taken from the World Ocean Atlas (WOA; Garcia et al., 2014). It is assumed that a fixed fraction

662   (σJ_{prod}) of phosphate uptake is converted into Dissolved Organic Phosphorus (DOP) which is a

663   source for J_{DOP} (equation A6). The phosphate not converted to DOP results in an instantaneous

664   downward flux of particulate organic phosphorus at Zc (equation A14). The decrease of flux

665   with depth due to remineralization is shown by a power law relationship as in equation A15. The

666   values of the constants a, κ, σ are 0.9, 0.2/year to 0.7/year, 0.67, respectively. The rate of

667   production is used to explain the formation of calcium carbonate cycle in surface waters

668   (equation A8) and its export is given by equation A16, where R is the rain ratio, a constant molar

669   ratio of exported particulate organic carbon to the exported calcium carbonate flux at Zc. The

670   exponential decrease of calcium carbonate flux with scale depth d is given by equation A17. The

671   biological source or sink of dissolved inorganic carbon (DIC) and alkalinity (ALK) is explained

672   through equations A9 and A10, respectively. Where the values of rain ratio (R) is taken as 0.07

673   and the Redfield ratio, $r_{C:P} = 117$, and $r_{N:P} = 16$ and scale depth d is chosen as 3500m.

674

Biological and Solubility Pump calculations

676   The biological effect on DIC is calculated from Louanchi et al., (1996). The tendency of DIC

677   due to biomass production and calcite formation in the production zone is expressed as below.

678
$$\left(\frac{\partial DIC}{\partial t}\right)_b = \left(\frac{\partial PO_4}{\partial t}\right)_b \times R_{C:P} - J_{Ca} \qquad (A18)$$

679   The total tendency of DIC in the production zone is:

680
$$\left(\frac{\partial DIC}{\partial t}\right)_{total} = \left(\frac{\partial DIC}{\partial t}\right)_b + \int_x \int_y F dx\, dy \qquad (A19)$$

681   where $\left(\frac{\partial DIC}{\partial t}\right)_b$ is the evolution of DIC due to the impact of biology (i.e., biological pump). The

682   first term in the R.H.S of Equation A18 is the rate of change of phosphate resulting from

683   photosynthesis and respiration in the model (i.e., J_{po4} in this case) multiplied by the carbon to

684   phosphorous Redfield ratio ($R_{C:P}$ = 117:1) and J_{Ca} represents the calcite formation in the model

685   (see Equation A8 & A16). The solubility pump is calculated as the surface integral of the flux F

686   (Louanchi et al., 1996).

687

688   **Appendix B**

689   In order to compare our model production of organic phosphorous to the curve of Ryther et al.,

690   (1956) we have merely scaled our total production to "relative photosynthesis", which is,

691   according to Ryther et al., (1956) an index between 0 and 1 indicating the strength of production

692   estimated as P_l/P_{max}. Here P_l is the photosynthesis at each intensity (of light) of different species

693   and P_{max} is the maximum photosynthesis observed in the same control experiment. The curve

694   between relative photosynthesis and light intensity shows the relation between photosynthetic

695   activity and light in marine phytoplankton. Since our method relates biological production to a

696   function of light (limitation) by Chl-a attenuation, it is the best curve to cross-compare our

697   results. In this case we scaled our total biological production within Zc into relative values

698   between 0-1 by P_l/P_{max}. in which P_l is taken as the individual grid cell biological component of

699   organic phosphorus production and P_{max} is the maximum production available in the domain at

700   any given instant. All the grid points are quite similar to the curve of Ryther et al., (1956) as

701   shown in Figure 2.

702

Acknowledgements

Thanks to two anonymous reviewers and the editor (Marilaure Grégoire) for comments. Sreeush M. G. sincerely acknowledges the fellowship support from Indian Institute of Tropical Meteorology (IITM) to carry out the study. The OCMIP-II routines were taken from (http://ocmip5.ipsl.jussieu.fr/OCMIP/). GFDL data for OTTM is taken from (http://data1.gfdl.noaa.gov/nomads/forms/assimilation.html). Takahashi data is taken from (http://www.ldeo.columbia.edu/res/pi/CO2/) and SeaWiFS data is obtained from the National Aeronautics and Space Administration (NASA) Ocean Color Website (http://oceancolor.gsfc.nasa.gov/). The computations were carried out in High-Performance Computing (HPC) facility of Ministry of Earth Sciences (MoES), IITM.

722   **References**

723   Anderson, L. A., Sarmiento, J. L.: Global ocean phosphate and oxygen simulations, Global

724   Biogeochem. Cycles, 9, 621-636, doi:10.1029/95GB01902, 1995.

725   Asselin, R.: Frequency filter for time integrations, Mon. Wea. Rev., 100, 487–490, doi:

726   10.1175/1520-0493, 1972.

727   Banse, K., McClain, C. R.: Winter blooms of phytoplankton in the Arabian Sea as observed by

728   the Coastal Zone Color Scanner, Mar. Ecol. Prog. Ser, 34, 201 – 211, 1986.

729   Banse, K.: Seasonality of phytoplankton chlorophyll in the central and northern Arabian Sea,

730   Deep Sea Res., 34, 713 – 723, doi:10.1016/0198-0149, 1987.

731   Barber, R. T., Marra. J., Bidigare. R. C., Codispoti. L. A., Halpern. D., Johnson. Z., Latasa. M.,

732   Goericke. R., and Smith. S. L.: Primary productivity and its regulation in the Arabian Sea during

733   1995, Deep. Sea. Res. pt. II, 48, 1127 – 1172. doi:10.1016/S0967-0645, 2001.

734   Bates, N. R., Pequignet. A. C., and Sabine. C. L.: Ocean carbon cycling in the Indian Ocean: 2.

735   Estimates of net community production, Global Biogeochem. Cycles., 20, GB3021,

736   doi:10.1029/2005GB002492, 2006.

737   Bauer, S., Hitchcock, G. L., Olson, D. B.: Influence of monsoonally-forced Ekman dynamics

738   upon surface-layer depth and plankton biomass distribution in the Arabian Sea, Deep Sea Res.,

739   38, 531 – 553, doi:10.1016/0198-0149, 1991.

740   Behrenfeld, M. J., Falkowski. P. G.: Photosynthetic rates derived from satellite-based

741   chlorophyll concentration, Limnol. Oceanogr., 42, 1 – 20, doi: 10.4319/lo.1997.42.1.0001, 1997.

742 Boyd, P. W., Rynearson, T. A., Armstrong, E. A., Fu. F., Hayashi. K. and co-authors.: Marine

743 Phytoplankton Temperature versus growth responses from polar to tropical waters – outcome of

744 a scientific community-wide study, PLoS ONE 8(5)., e63091,

745 Doi:10.1371/journal.phone.0063091, 2013.

746 Brock, J C., McClain, C. R.: Interannual variability of the southwest monsoon phytoplankton

747 bloom in the north-western Arabian Sea, J. Geophys. Res., 97(C1), 733 – 750,

748 doi/10.1029/91JC02225, 1992a.

749 Brock, J. C., McClain, C. R., Hay, W. W.: A southwest monsoon hydrographic climatology for

750 the northwestern Arabian Sea, J. geophys. Res., 97(C6), 9455 – 9465, doi: 10.1029/92JC00813,

751 1992b.

752 Brock, J. C., McClain, C. R., Luther, M. E., Hay, W. W.: The phytoplankton bloom in the

753 northwestern Arabian Sea during the southwest monsoon of 1979, J. Geophys. Res., 96(C11),

754 623 – 642, doi: 10.1029/91JC01711, 1991.

755 Brock. J., Sathyendranath. S., and Platt. T.: Modelling the seasonality of subsurface light and

756 primary production in the Arabian Sea, Mar. Eco. Prog. Ser., 101, 209 – 221, 1993.

757 Bruce, J. G.: Some details of upwelling off the Somali and Arabian coasts, J. Mar. Res., 32, 419

758 – 423, 1974.

759 Bryan. K., Lewis, L. J.: A water mass model of the world ocean, J. Geophys. Res., 84, 2503 –

760 2517, doi: 10.1029/JC084iC05p02503, 1979.

761 Chang, Y. S., Zhang. S., Rosati. A., Delworth. T., Stern. W. F.: An assessment of oceanic

762 variability for 1960-2010 from the GFDL ensemble coupled data assimilation, Clim. Dyn., 40,

763 775 – 803, doi: 10.1007/s00382-012-1412-2, 2012.

764 Christian J. R., Verschall M. A., Murtugudde R., Busalacchi A. J., McClain C. R.:

765 Biogeochemical modeling of the tropical Pacific Ocean. II: Iron biogeochemistry, Deep Sea

766 Res., 49, 545 – 565, doi:10.1016/S0967-0645, 2001.

767 Colwell, R. R.: Global climate and infectious disease: the cholera paradigm, Science., 274(5295),

768 2025 – 2031, doi: 10.1126/science.274.5295.2025, 1996.

769 Dickson, A. G., and F. J. Millero.: A comparison of the equilibrium constants for the dissociation

770 of carbonic acid in seawater media, Deep-Sea Res., 34, 1733 – 1743, 1987.

771 Dilmahamod A. F., Hermes. J. C., Reason C. J. C.: Chlorophyll-a variability in the Seychelles-

772 Chagos Thermocline Ridge: Analysis of a coupled biophysical model, J. of. Mar. Sys., 154, 220

773 – 232, doi:10.1016/j.jmarsys.2015.10.011, 2016.

774 Doney S. C., and co-authors.: Evaluating global ocean carbon models: The importance of

775 realistic physics, Glob. Biogeochem. Cycles, 18, doi:10.1029/2003GB002150, 2004.

776 Eppley, R. W., Peterson. B. J.: Particulate organic matter flux and planktonic new production in

777 the deep ocean, Nature, 282, 677-680, doi:10.1038/282677a0, 1979.

778 Eppley, R. W.: Temperature and phytoplankton growth in the sea, Fish. Bull., 70, 1063 – 1085,

779 1972.

780 Falkowski, P. G., E. A. Laws, R. T. Barber, and J. W. Murray: phytoplankton and their role in

781 the primary, new and export production, In: Fasham M.J.R (eds) Ocean Biogeochemistry, Global

782 Change – The IGBP series (closed). Springer, Berlin, Heidelberg, doi:

783 https://doi.org/10.1007/978-3-642-55844-3_5, 2003.

784 Feely, R. A., Sabine, C. L., Takahashi, T., Wanninkhof, R.: Uptake and Storage of Carbon

785 Dioxide in the Ocean: The Global CO_2 Survey, Oceanography., 14(4), 18–32,

786 doi:10.5670/oceanog.2001.03, 2001.

787 Friedrichs, M. A. M., and co-authors.: Assessment of skill and portability in regional

788 biogeochemical models: role of multiple planktonic groups, J. Geophy. Res., 112, doi:

789 10.1029/2006JC003852, 2007.

790 Friedrichs, M. A. M., Hood, R. R., Wiggert, J. D.: Ecosystem complexity versus physical forcing

791 quantification of their relative impact with assimilated Arabian Sea data, Deep Sea Res., 53, 576-

792 600, doi:10.1016/j.dsr2.2006.01.026, 2006.

793 Garcia, H. E., R. A. Locarnini, T. P. Boyer, J. I. Antonov, O.K. Baranova, M.M. Zweng, J.R.

794 Reagan, D.R. Johnson.: World Ocean Atlas 2013, Volume 4: Dissolved Inorganic Nutrients

795 (phosphate, nitrate, silicate), S. Levitus, Ed., A. Mishonov Technical Ed.; NOAA Atlas NESDIS

796 76, 25 pp, 2014.

797 Gattuso, J. P., B. Gentili, C. M. Duarte, J. A. Kleypas, J. J. Middelburg, and D. Antoine.: Light

798 availability in the coastal ocean: Impact on the distribution of benthic photosynthetic organisms

799 and their contribution to primary production, Biogeosciences, 3, 489 – 513, doi:10.5194/bg-3-

800 489-2006, 2006.

801 Gent, P. R., McWilliams. J. C.: Isopycnal mixing in ocean circulation models, J. Phys.

802 Oceanogr., 20, 150 – 155, doi: 10.1175/15200485, 1990.

803   Harwell, C., Kim, K., Burkholder, J., Colwell, R., Epstein, P. R., Grimes, D., Hofmann, E. E.,

804   Lipp, E. K., Osterhaus, A., and Overshreet, R. M.: Emerging marine diseases-climate links and

805   anthropogenic factors, Science., 285(5433), 1505 – 1510, doi: 10.1126/science.285.5433.1505,

806   1999.

807   Jerlov N. G.: Marine optics, Second ed., Elsevier, pp 231, 1976.

808   Jung, E., and Kirtman. B. P.: ENSO modulation of tropical Indian ocean subseasonal variability,

809   Geophys. Res. Lett., 43, doi: 10.1002/2016GL071899, 2016.

810   Keeling, C. D., Whorf, T. P., Wahlen, M., and van der plicht, J.: Interannual extremes in the rate

811   of rise of atmospheric carbon dioxide since 1980, Nature, 375, 666 – 670, 1995.

812   Key, R. M., et al,.: A global ocean carbon climatology: Results from Global Data Analysis

813   Project (GLODAP), Global Biogeochem. Cycles, 18, GB4031, doi:10.1029/2004GB002247,

814   2004

815   Krey, J., Bahenerd, B.: Phytoplankton production atlas of the international Indian Ocean

816   expedition, Institut fur Meereskundeander Universitat Kiel, Kiel, German, 1976.

817   Large, W. G., McWilliams, J. C., Doney, S. C.: Oceanic vertical mixing: A review and a model

818   with a nonlocal boundary layer parameterization, Rev. Geophys., 32, 363 – 403, doi:

819   10.1029/94RG01872, 1994.

820   Laws, E. A., P. G. Falkowski, W.O. Smith, Jr., H. Ducklow and J. J. McCarthy: Temperature

821   effects on export production in the open ocean, Global Biogeochem. Cycles, 14, 1231 – 1246,

822   2000.

823   Le Quere, C., Orr, J. C., Monfray, P., Aumont, O.: Interannual variability of the oceanic sink of

824   CO_2 from 1979 through 1997, Global Biogeochem. Cycles., 14, p1247 – 1265, doi:

825   10.1029/1999GB900049, 2000.

826   Lee, P. F., Chen, I. C., Tzeng. W. N.: Spatial and Temporal distributions patterns of bigeye tuna

827   (Thunnusobsesus) in the Indian Ocean, Zoological studies-Taipei-, 44(2), 260, 2005.

828   Lehodey .P., Senina I., Sibert. J., Bopp. L., Calmettes B., Hampton .J., Murtugudde. R.:

829   Preliminary forecasts of Pacific bigeye tuna population trends under the A2 IPCC scenario, Prog

830   in Oceanography., 86, 302 – 315, doi:10.1016/j.pocean.2010.04.021, 2010.

831   Liao, X., Zhan, H., Du, Y.: Potential new production in two upwelling regions of the Western

832   Arabian Sea: Estimation and comparison, J. Geophys. Res. Oceans., 121,

833   doi:10.1002/2016JC011707, 2016.

834   Lopez-Urrutia, A., E. San Martin, R. P. Harris, and X. Irigoien.: Scaling the metabolic balance of

835   the oceans, Proc. Natl. Acad. Sci. U.S.A., 103, 8739-8744,doi:10.1073/pnas.0601137103, 2006.

836   Louanchi. F., N. Metzl., and Alain Poisson.: Modelling the monthly sea surface f_{CO2} fields in the

837   Indian Ocean, Marine Chemistry, 55, 265 – 279, 1996.

838   Marra, J. F., Veronica P. Lance, Robert D. Vaillancourt, Bruce R. Hargreaves.: Resolving the

839   ocean's euphotic zone, Deep Sea. Res. pt. I., 83, 45 -50, doi:10.1016/j.dsr.2013.09.005, 2014.

840   Matsumoto K., Tokos. K. S., Price., A. R., Cox. S. J.: First description of the Minnesota Earth

841   System Model for Ocean biogeochemistry (MESMO 1.0), Geosci. Model Dev., 1, 1-15,

842   doi:10.5194/gmd-1-1-2008, 2008.

843 McCreary, J., Murtugude, R., Vialard, J., Vinayachandran, P., Wiggert, J. D., Hood, R. R.,

844 Shankar, D., Shetye, S.: Biophysical processes in the Indian Ocean, Indian Ocean

845 Biogeochemical Processes and Ecological Variability., 9 − 32, doi: 10.1029/GM185, 2009.

846 Mehrbach, C., C. H. Culberson, J. E. Hawley, and R. M. Pytkowicz.: Measurement of the

847 apparent dissociation constants of carbonic acid in seawater at atmospheric pressure, Limnol.

848 Oceanogr., 18, 897 − 907, 1973.

849 Moisan, J. R., Moisan, A. T., Abbott, M. R.: Modelling the effect of temperature on the

850 maximum growth rates of phytoplankton populations, Eco. Modelling., 153, 197-215,

851 doi:10.1016/S0304-3800(02)00008, 2002.

852 Morel, A.: Optical modeling of the upper ocean in relation to its biogenous matter content (Case

853 1 Waters), J. Geophys. Res., 93, 10479-10, 768, doi: 10.1029/JC093iC09p10749, 1988.

854 Murtugudde R., McCreary J. P., Busalacchi, A. J.: Oceanic processes associated with anomalous

855 events in the Indian Ocean with relevance to 1997-1998, J. Geophys. Res., 105, 3295-3306, doi:

856 10.1029/1999JC900294, 2000.

857 Murtugudde, R. G., S. R. Signorini, J. R. Christian, A. J. Busalacchi, C. R. McClain, and J.

858 Picaut.: Ocean color variability of the tropical Indo-Pacific basin observed by SeaWiFS during

859 1997 − 1998, J. Geophys. Res., 104(C8), 18351 − 18366, doi.10.1029/1999JC900135, 1999a.

860 Murtugudde, R., Busalacchi, A. J.: Interannual variability of the dynamics and thermodynamics

861 of the tropical Indian Ocean, J. Clim. 12, 2300-2326, doi:10.1175/1520-0442, 1999b.

862 Murtugudde, R., Seager, R., Thoppil, P.: Arabian Sea response to monsoon variations,

863 Paleoceanography., 22, PA4217, doi:10.1029/2007PA001467, 2007.

864   Najjar, R. G., Keeling, R. F.: Analysis of the mean annual cycle of the dissolved oxygen

865   anomaly in the world ocean, J. Mar. Res., 55, 117 – 151, doi:10.1357/0022240973224481, 1997.

866   Najjar, R. G., Orr, J. C.: Design of OCMIP-2 simulations of chlorofluorocarbons, the solubility

867   pump and common biogeochemistry, http://www.ipsl.jussieu.fr/OCMIP/., 1998.

868   Najjar, R. G., Sarmiento, J. L., Toggweiler, J. R.: Downward transport and fate of organic matter

869   in the ocean: simulations with a general circulation model, Global Biogeochem. Cycles., 6, 45-

870   76, doi/10.1029/91GB02718, 1992.

871   Naqvi, S. W. A., Moffett, J. W., Gauns, M. U., Narvekar, P. V., Pratihary, A. K., Naik, H.,

872   Shenoy, D. M., Jayakumar, D. A., Goepfert, T. J., Patra, P. K., Al-Azri, A., and Ahmed, S. I.:

873   The Arabian Sea as a high-nutrient, low-chlorophyll region during the late Southwest Monsoon,

874   Biogeosciences., 7, 2091-2100, doi:10.5194/bg-7-2091-2010, 2010.

875   Naqvi, S., Naik, H., Narvekar, P.: The Arabian Sea, in Biogeochemistry, edited by K. Black and

876   G. Shimmield, pp. 156 – 206, Blackwell, Oxford, 2003.

877   Orr, J. C., and co-authors.: Anthropogenic ocean acidification over the twenty-first century and

878   its impact on calcifying organisms, Nature, 437, 681 – 686, doi:10.1038/nature04095, 2005.

879   Orr, J. C., and co-authors.: Estimates of anthropogenic carbon uptake from four three-

880   dimensional global ocean models, Glob. Biogeochem. Cycles., 15, p43 – 60, doi:

881   10.1029/2000GB001273, 2001.

882   Orr, J. C., Aumont, O., Bopp, L., Calderia, K., Taylor, K., et. al.: Evaluation of seasonal air-sea

883   CO2 fluxes in the global carbon cycle models, International open Science conference (Paris, 7-

884   10 Jan. 2003), 2003.

885   Osawa, T., Julimantoro, S.: Study of fishery ground around Indonesia archipelago using remote

886   sensing data, International archives of the Photogrammetry, Remote sensing and spatial

887   information science., vol XXXVIII, part-8, 2010.

888   Parsons, T. R., Takahashi, M., Habgrave, B.: In Biological Oceanographic Processes, 3rd ed.,

889   330pp., Pergamon Press, New York, doi: 10.1002/iroh.19890740411, 1984.

890   Prasanna Kumar, .S., Muraleedharan, P. M., Prasad, T. G., Gauns, M., Ramaiah, N., de Souza, S.

891   N., Sardesai, S., Madhupratap, M.: Why is the Bay of Bengal less productive during summer

892   monsoon   compared   to   the   Arabian   Sea?,   Geophys.   Res.   Lett.,   29(24),   2235,

893   doi:10.1029/2002GL016013, 2002.

894   Prasanna Kumar, S., Roshin, P. R., Narvekar, J., Dinesh Kumar, P., Vivekanandan, E.: What

895   drives the increased phytoplankton biomass in the Arabian Sea?, Current Science, 99(I), 101 –

896   106, 2010.

897   Prassana Kumar. S, Ramaiah. N, Gauns. M., Sarma V. V. S. S., Muraleedharan. P. M.,

898   RaghuKumar. S., Dileep Kumar., Madhupratap. M.: Physical forcing of biological productivity

899   in the Northern Arabian Sea during the Northeast Monsoon, Deep Sea Res. Pt. II., 48, 1115-

900   1126, doi:10.1016/S0967-0645(00)00133-8, 2001.

901   Praveen, V., Ajayamohan, R. S., Valsala, V., Sandeep, S.: Intensification of upwelling along

902   Oman coast in a warming scenario, Geophys. Res. Lett., 43, doi:10.1002/2016GL069638, 2016.

903   Press, W. H., and others: Numerical Recipes in FORTRAN. Cambridge University Press,

904   Cambridge, England, 1996.

905   Qasim, S. Z.: Biological productivity of the Indian Ocean, J. Mar. Sci., 6, 122 – 137, 1977.

906   Qasim, S. Z.: Oceanography of Northern Arabian Sea, Deep Sea Res., 29(9A), 1041 − 1068,

907   doi:10.1016/0198-0149(82)90027-9, 1982.

908   Redi, M.: Oceanic isopycnal mixing by coordinate rotation, J. Phys. Oceanogr., 12, 1154 − 1158,

909   doi: 10.1175/1520-0485, 1982.

910   Regaudie-de-Gioux, A., and C. M. Duarte.: Compensation irradiance for planktonic community

911   metabolism   in   the   ocean,   Global   Biogeochem.   Cycles,   24,   GB4013,

912   doi:10.1029/2009GB003639, 2010.

913   Roxy, M. K., Modi, A., Murtugudde, R., Valsala, V., Panickal, S., Prasanna Kumar, S.,

914   Ravichandran, M., Vichi, M., Levy, M.: A reduction in marine primary productivity driven by

915   rapid warming over the tropical Indian Ocean, 43, 826 − 833, J. Geophys. Res. Letters.,

916   doi:10.1002/2015GL066979, 2015.

917   Ryther, J., Menzel, D.: On the production, composition, and distribution of organic matter in the

918   Western Arabian Sea, Deep Sea Research and Oceanographic Abstracts., 12(2), 199 -209.

919   doi:10.1016/0011-7471(65)90025-2, 1965.

920   Ryther, J.: Photosynthesis in the ocean as function of light Intensity, Limnol. Oceanogr., vol 1,

921   issue 1, doi: 10.4319/lo.1956.1.1.0061, 1956.

922   Sarma V. V. S. S.: Net plankton community production in the Arabian Sea based on O_2 mass

923   balance model, Glob. Biogeochem. Cycles., 18, GB4001, doi:10.1029/2003GB002198, 2004.

924   Sarma, V. V. S. S.: An evaluation of physical and biogeochemical processes regulating the

925   perennial suboxic conditions in the water column of the Arabian Sea, Global Biogeochem.

926   Cycles., 16, doi:10.1029/2001GB001461, 2002.

927   Sarmiento, J. L., and Gruber, N.: Ocean Biogeochemical Dynamics, Princeton University Press,

928   New Jersey, 2006.

929   Sarmiento, J. L., Monfray. P., Maier-Reimer., Aumont, O., Murnane, R. J., Orr, J. C.: Sea-air

930   CO_2 fluxes and carbon transport: A comparison of three ocean general circulation models,

931   Global Biogeochem. Cycles., 14, p1267 – 1281. doi: 10.1029/1999GB900062, 2000.

932   Schott, F.: Monsoon response of the Somali current and associated upwelling, Prog.Oceanogr.,

933   12, 357 – 381, doi:10.1016/0079-6611(83)90014-9, 1983.

934   Smetacek, V., and Passow, U.: Spring bloom initiation and Sverdrup's critical depth model,

935   Limnol. Oceanogr., 35, 228 – 234, doi: 10.4319/lo.1990.35.1.0228, 1990.

936   Smith, L. S.: Understanding the Arabian Sea: Reflections on the 1994-1996 Arabian Sea

937   Expedition, Deep Sea Res. Pt. II., 48, 1385-1402, doi:10.1016/S0967-0645(00)00144-2, 2001.

938   Smith, R. L., Bottero, L. S.: On upwelling in the Arabian Sea. In Angel, M (ed) A voyage of

939   Discovery. Pergamon Press, New York, p. 291 – 304, 1977.

940   Smith, S. L., Codispoti, L. A.: Southwest monsoon of 1979: chemical and biological response of

941   Somali coastal waters. Science, 209, 597 – 600. doi:10.1126/science.209.4456.597, 1980.

942   Smith, S. L.: Biological indications of active upwelling in the northwestern Indian Ocean in 1964

943   and 1979, a comparison with Peru and northwest Africa, Deep Sea Res., 31, 951 – 967,

944   doi:10.1016/0198-0149(84)90050-5, 1984.

945   Susanto. R., Gordon, A. L., Zheng. Q.: Upwelling along the coasts of Java and Sumatra and its

946   relation to ENSO, J. Geophys. Res. Lett., 28, 1599-1602, doi: 10.1029/2000GL011844, 2001.

947   Swallow, J. C.: Some aspects of the physical oceanography of the Indian Ocean, Deep Sea Res.,

948   31, 639 – 650, doi:10.1016/0198-0149(84)90032-3, 1984.

949   Takahashi, T., Sutherland, S. C., Wanninkhof, R., Sweeney, C., Feely, R. A., Chipman, D. W.,

950   Hales, B., Friederich, G., Chavez, F., Sabine, C., et al.: Climatological mean and decadal

951   changes in surface ocean pCO_2 and net sea-air CO_2 flux over the global oceans. Deep Sea Res.,

952   Pt. II., 56, 554 – 557, doi:10.1016/j.dsr2.2008.12.009, 2009.

953   Valsala V., Maksyutov, S.: A short surface pathway of the subsurface Indonesian Throughflow

954   water from the Java Coast associated with upwelling, Ekman Transport, and Subduction. Int. J.

955   Oceanogr., 15, doi: 10.1155/2010/540743, 2010a.

956   Valsala V., Maksyutov, S.: Interannual variability of air-sea CO_2 flux in the north Indian Ocean,

957   Ocean Dynamics., 1 – 14, doi 10.1007/s10236-012-0588-7, 2013.

958   Valsala V., R. R. Rao.: Coastal Kelvin waves and dynamics of gulf of Aden eddies, Deep Sea

959   Res., Pt. I., 116, 174 – 186, https://doi.org/10.1016/j.dsr.2016.08.003, 2016.

960   Valsala, K. V., Maksyutov, S., Ikeda, M.: Design and Validation of an offline oceanic tracer

961   transport model for a carbon cycle study, J. clim., 21, doi: 10.1175/2007JCLI2018.1, 2008.

962   Valsala, V., Maksyutov, S., Murtugudde, R.: Interannual to Interdecadal Variabilities of the

963   Indonesian Throughflow Source Water Pathways in the Pacific Ocean, J. Phys. Oceanogr., 41,

964   1921–1940, doi: 10.1175/2011JPO4561.1, 2011.

965   Valsala, V., Maksyutov, S.: Simulation and assimilation of global **oc**ean pCO_2 and air-sea CO_2

966   fluxes using ship observations of surface ocean pCO_2 in a simplified biogeochemical model,

967   Tellus., 62B, doi: 10.1111/j.1600-0889.2010.00495, 2010b.

968   Valsala, V**.,** Murtugudde, R.: Mesoscale and Intraseasonal Air-Sea CO_2 Exchanges in the

969   Western Arabian Sea during Boreal Summer, Deep Sea Res. Pt. I, 103, 103-113,

970   doi:10.1016/j.dsr.2015.06.001, 2015.

971   Valsala, V**.,** Roxy, M., Ashok, K., Murtugudde, R.: Spatio-temporal characteristics of seasonal to

972   multidecadal variability of pCO_2 and air-sea CO_2 fluxes in the equatorial Pacific Ocean, J.

973   Geophys. Res., 119, 8987 – 9012, doi:10.1002/2014JC010212, 2014.

974   Valsala, V.: Different spreading of Somali and Arabian coastal upwelled waters in the northern

975   Indian Ocean: A case study. J. Phy. Oceanogr., 803 – 816, doi: https://doi.org/10.1007/s10872-

976   009-0067-z, 2009.

977   Vialard, J. and co-authors.: Air-Sea Interactions in the Seychelles-Chagos Thermocline Ridge

978   Region, BAMS, doi:10.1175/2008BAMS2499.1, 2009.

979   Vinayachandran P. N., Yamagata, T.: Monsoon Response of the Sea around Sri Lanka:

980   Generation of Thermal Domes and Anticyclonic Vortices, J. Phy. Oceano., 28, 1946 – 1960, doi:

981   10.1175/1520-0485, 1998.

982   Vinayachandran, P. N., Chauhan, P., Mohan, M., Nayak, S.: Biological response of the sea

983   around Sri Lanka to summer monsoon, Geophys. Res. Lett., 31, L0I302,

984   doi:10.1029/2003GL018533, 2004.

985   Wang .X. J., Behrenfeld. M., Le Borgne .R., Murtugudde .R., and Boss. E.: Regulation of

986   phytoplankton carbon to chlorophyll ratio by light, nutrients and temperature in the equatorial

987   Pacific Ocean: a basin-scale model. Biogeosciences., 6, 391 – 404, doi:10.5194/bg-6-391-2009,

988   2009.

989 Weiss, R. F.: Carbon dioxide in water and seawater: The solubility of a non-ideal gas, Mar.

990 Chem., 2, 203-215, 1974.

991 Wiggert J. D., Jones. B. H., Dickey .T D., Brink .K. H., Weller .R .A., Marra. J., Codispoti. L.

992 A.: The Northeast Monsoon's impact on mixing, phytoplankton biomass and nutrient cycling in

993 the Arabian Sea, Deep Sea Res. Pt. II, 47, 1353-1385, doi:10.1016/S0967-0645(99)00147-2,

994 2000.

995 Wiggert, J. D., Hood, R. R., Banse, K., Kindle, J. C.: Monsoon-driven biogeochemical processes

996 in the Arabian Sea, Progr. Oceanogr., 65, 176-213, doi:10.1016/j.pocean.2005.03.008, 2005.

997 Wiggert. J. D., Murtugudde, R. G., Christian J. R.: Annual ecosystem variability in the tropical

998 Indian Ocean: results of a coupled bio-physical ocean general circulation model, Deep Sea Res.

999 Pt. II., 53, 644-676, doi:10.1016/j.dsr2.2006.01.027, 2006.

1000 Xie, S. P., Annamalai, H., Schott, F. A., McCreary Jr. J. P.: Structure and mechanism of south

1001 Indian ocean climate variability, J. clim., 15, 864 – 878, doi: 10.1175/1520-0442, 2002.

1002 Xing W., Xiaomei. L., Haigang Z., Hailong. L.: Estimates of potential new production in the

1003 Java-Sumatra upwelling system, Chinese Journal of Oceanology and Limnology., 30, 1063-

1004 1067, doi:10.1007/s00343-012-1281, 2012.

1005 Yamanaka, Y., Yoshie, N, Masahiko Fujii, Maka .N. Aita and Kishi. M. J.: An Ecosystem

1006 coupled with Nitrogen-Silicon-Carbon cycles applied to station A7 in the Northwestern Pacific,

1007 J. of Oceanogr., 60, p227-241, doi: 10.1023/B:JOCE.0000038329.91976.7d, 2004.

1008   Zhou X., Weng. E., Luo., Y.: Modelling patterns of nonlinearity in the ecosystem responses to

1009   temperature, CO_2 and precipitation changes, Eco. Appli., 18, 453 – 466, doi: 10.1890/07-0626.1,

1010   2008.

1011

Table: 1 WAS = Western Arabian Sea, SLD = Sri Lanka Dome, SC = Sumatra Coast, SCTR = Seychelles-Chagos Thermocline Ridge. JJAS mean and the climatological annual mean of CO_2 flux from Takahashi observations, constZc, and varZc simulations. Units are mol m^{-2} yr^{-1}.

| Regions | CO_2 flux (mol m^{-2} yr^{-1}) | | | | | |
| | JJAS Mean | | | Annual Mean | | |
	OBS	constZc	varZc	OBS	constZc	varZc
WAS	1.99	1.44 ± 0.2	2.31 ± 0.4	0.94	0.80 ± 0.1	1.07 ± 0.2
SLD	1.79	-0.008 ±0.2	0.24 ± 0.09	0.8	-0.02 ± 0.1	0.10 ± 0.2
SC	0.31	0.60 ± 0.5	1.51 ± 1.01	0.21	0.21 ± 0.3	0.53 ± 0.5
SCTR	0.82	-0.32 ± 0.3	-0.05 ± 0.4	0.55	-0.02 ± 0.1	-0.07 ± 0.2

Table: 2 Same as Table 1, but for pCO$_2$. Units are µatm.

| Regions | pCO$_2$ (µatm) | | | | | |
| | JJAS Mean | | | Annual Mean | | |
	OBS	constZc	varZc	OBS	constZc	varZc
WAS	397.58	389.18 ± 3.7	399.95 ± 5.01	394.69	389.62 ± 3.9	391.19 ± 4.7
SLD	382.44	371.67 ± 6.04	379.24 ± 8.9	380.21	370.76 ± 6.1	374.94 ± 9.6
SC	372.52	382.36 ± 12.7	402.14 ± 21.8	372.69	374.65 ± 9.3	381.76 ± 13.6
SCTR	377.18	365.71 ± 5.08	370.72 ± 7.4	379.89	372.69 ± 4.7	369.00 ± 5.4

Table: 3 JJAS mean and the climatological annual mean of export production from satellite-derived Net Primary Production data, constZc, and varZc simulations. Units are g C m^{-2} yr^{-1}.

Regions	Export Production (g C m^{-2} yr^{-1})					
	JJAS Mean			Annual Mean		
	OBS	constZc	varZc	OBS	constZc	varZc
WAS	123.57	84.81 ± 16.04	147.19 ± 23.8	94.31	77.41 ± 15.1	122.54 ± 25.2
SLD	51.54	167.71 ± 59.04	151.51 ± 46.4	43.25	144.43 ± 49.8	156.08 ± 43.8
SC	58.87	260.11 ± 104.7	310.03 ± 99.5	54.53	172.52 ± 72.4	215.52 ± 70.8
SCTR	51.08	57.39 ± 14.2	99.23 ± 21.8	40.45	55.15 ± 17.9	80.35 ± 26.04

Table: 4 Model derived values for New production. Units are g C m^{-2} yr^{-1}.

Regions	New Production (g C m^{-2} yr^{-1})					
	JJAS Mean			Annual Mean		
	OBS	constZc	varZc	OBS	constZc	varZc
WAS	--	150.84 ± 27.9	133.03 ± 19.5	--	108.43 ± 23.4	81.47 ± 15.7
SLD	--	141.93 ± 64.1	77.78 ± 27.6	--	111.05 ± 71.1	50.37 ± 26.3
SC	--	63.64 ± 30.9	78.11 ± 29.1	--	56.69 ± 43.3	54.58 ± 23.3
SCTR	--	12.17 ± 16.3	13.32 ± 18.6	--	13.74 ± 15.5	12.94 ± 13

Table 5: Biological pump impact over DIC in the model due to constZc and varZc simulations for JJAS and annual mean.

| Regions | Biological Pump (g C m^{-2} yr^{-1}) | | | |
| | constZc | | varZc | |
	JJAS Mean	Annual Mean	JJAS Mean	Annual Mean
WAS	45.18 ± 14.8	45.49 ± 14.38	151.7 ± 23.8	126.67 ± 24.3
SLD	89.39 ± 58.1	108.65 ± 48.6	156.07 ± 48.4	161.15 ± 43.5
SC	235.54 ± 95.4	155.21 ± 67.4	319.16 ± 94.9	222.92 ± 68.7
SCTR	30.49 ± 13.4	26.81 ± 16.8	103.13 ± 19.6	83.98 ± 23.6

Table 6: Same as Table 5, But for Solubility pump.

| Regions | Solubility Pump (g C m^{-2} yr^{-1}) | | | |
| | constZc | | varZc | |
	JJAS Mean	Annual Mean	JJAS Mean	Annual Mean
WAS	17.29 ± 3.5	9.63 ± 2.1	27.72 ± 4.8	12.92 ± 2.7
SLD	-0.09 ± 2.4	-0.32 ± 2.3	2.9 ± 3.5	1.31 ± 3.5
SC	7.22 ± 6.9	2.56 ± 3.8	18.17 ± 12.1	6.43 ± 6.0
SCTR	-3.95 ± 3.7	-0.35 ± 2.3	-0.61 ± 5.3	-0.86 ± 2.8
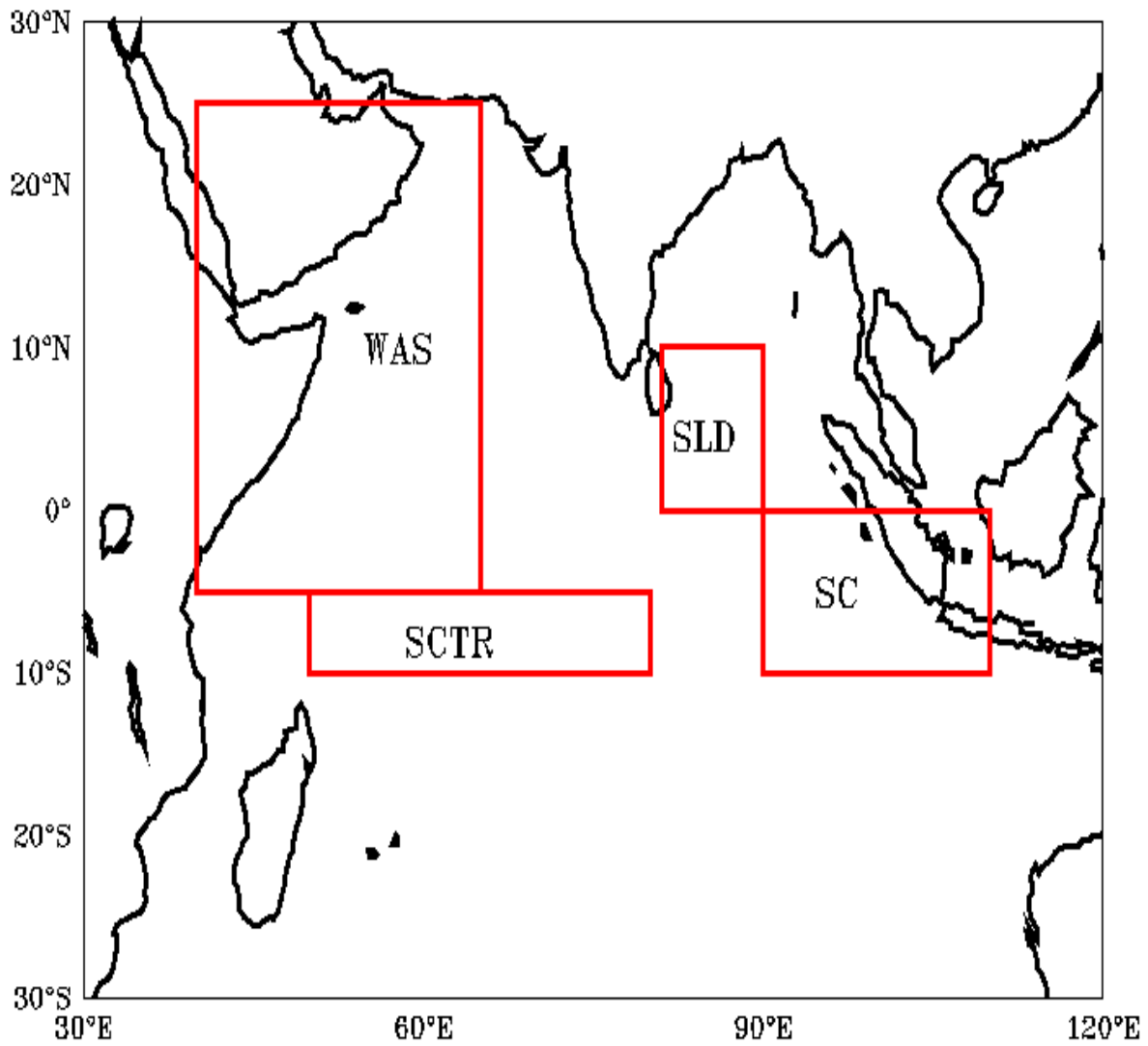
Figure 1: Red boxes shows the study regions (1) WAS (Western Arabian Sea, 40°E:65°E, 5°S:25°N) (2) SLD (Sri Lanka Dome, 81°E:90°E, 0°:10°N) (3) SC (Sumatra Coast, 90°E:110°E, 0°:10°S) and (4) SCTR (Seychelles-Chagos Thermocline Ridge, 50°E:80°E, 5°S:10°S).
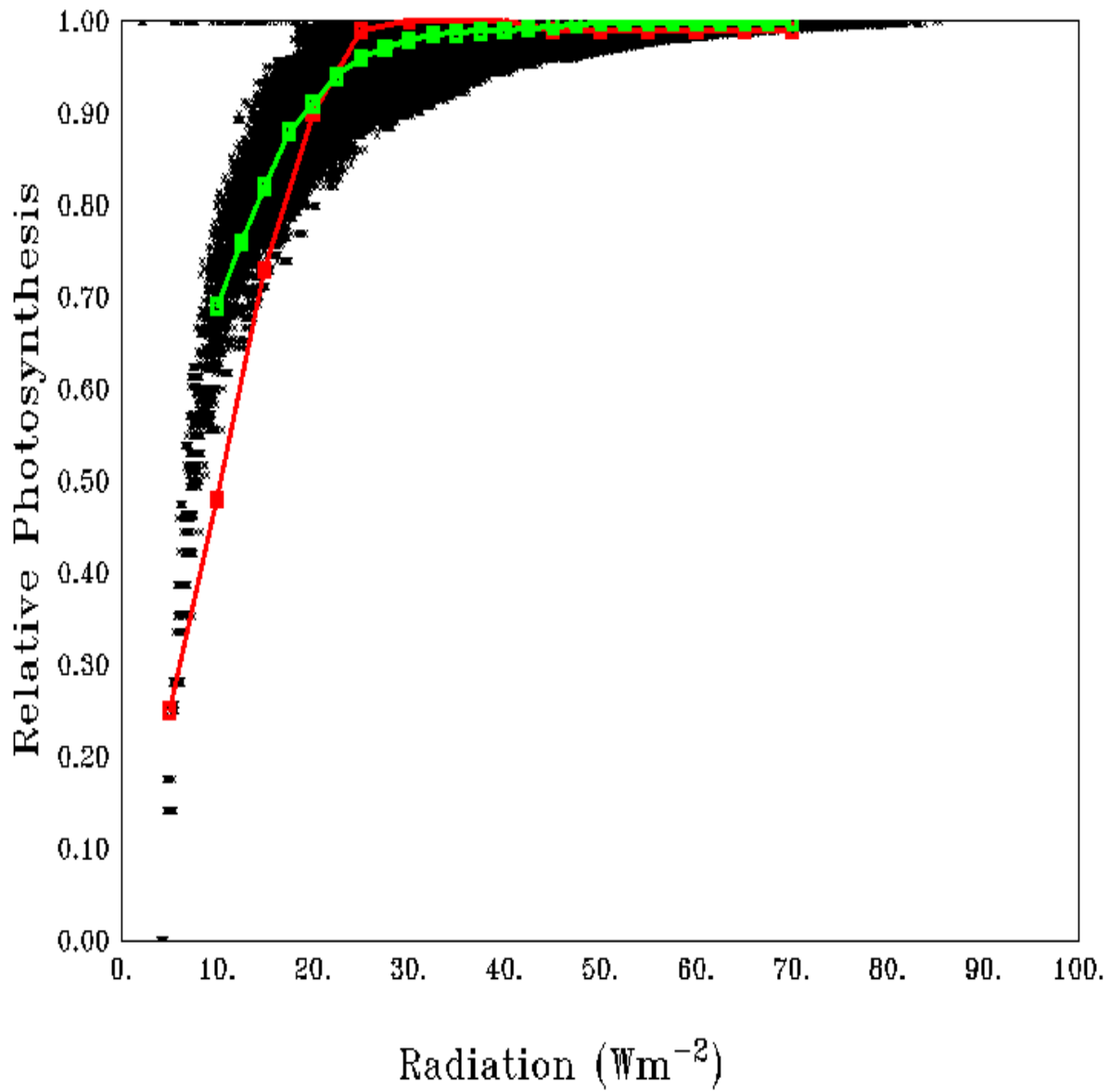
Figure 2: Scatter of average relative photosynthesis versus different light intensities in the model (black dots) and its mean (green curve). The red curve shows the theoretical P – I curve from Parsons et al., (1984).
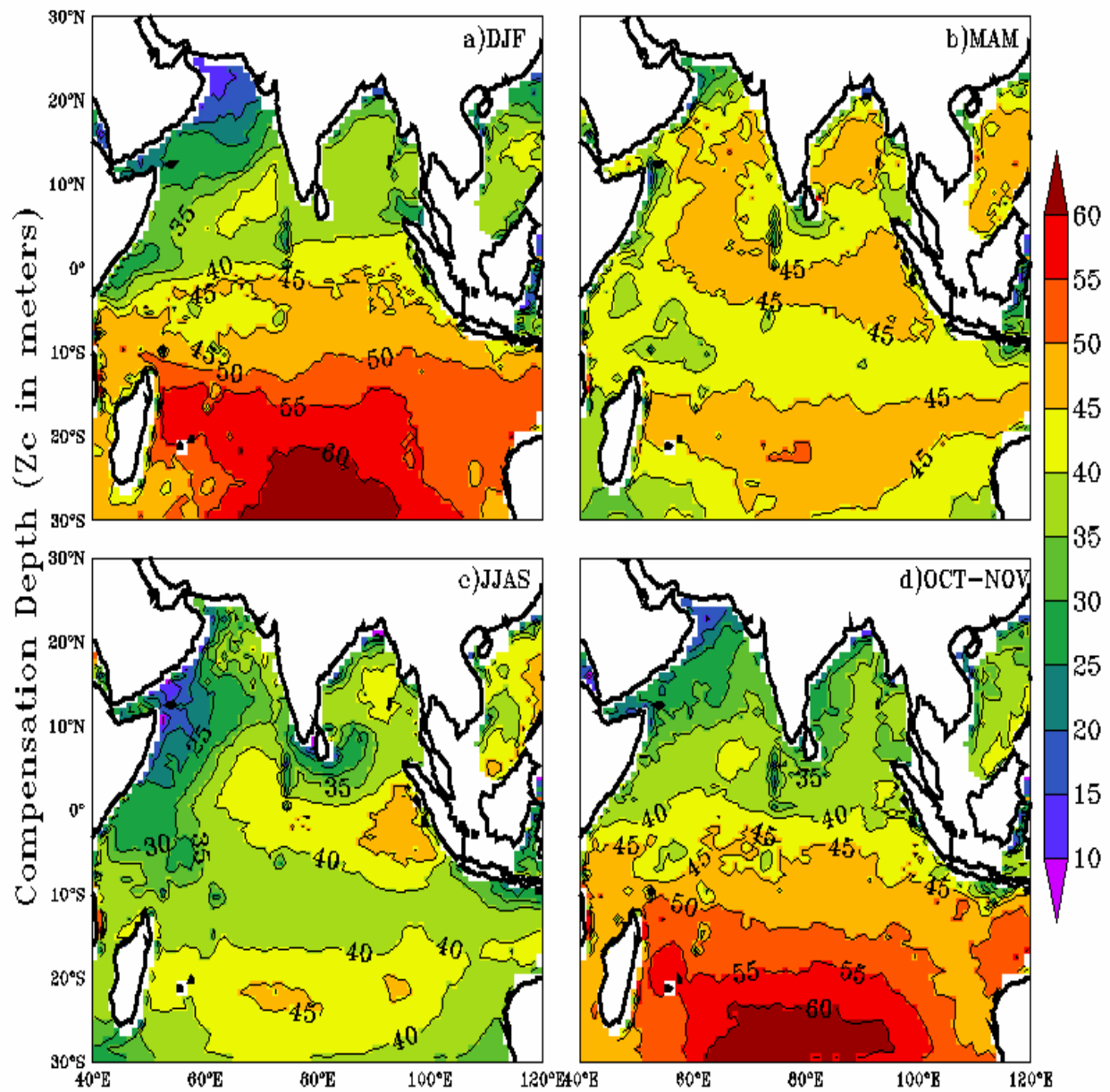
Figure 3: Seasonal-mean maps of varying compensation depth (varZc), (a) December to February (DJF), (b) March to May (MAM), (c) June to September (JJAS), (d) October to November (ON). Units are meters.
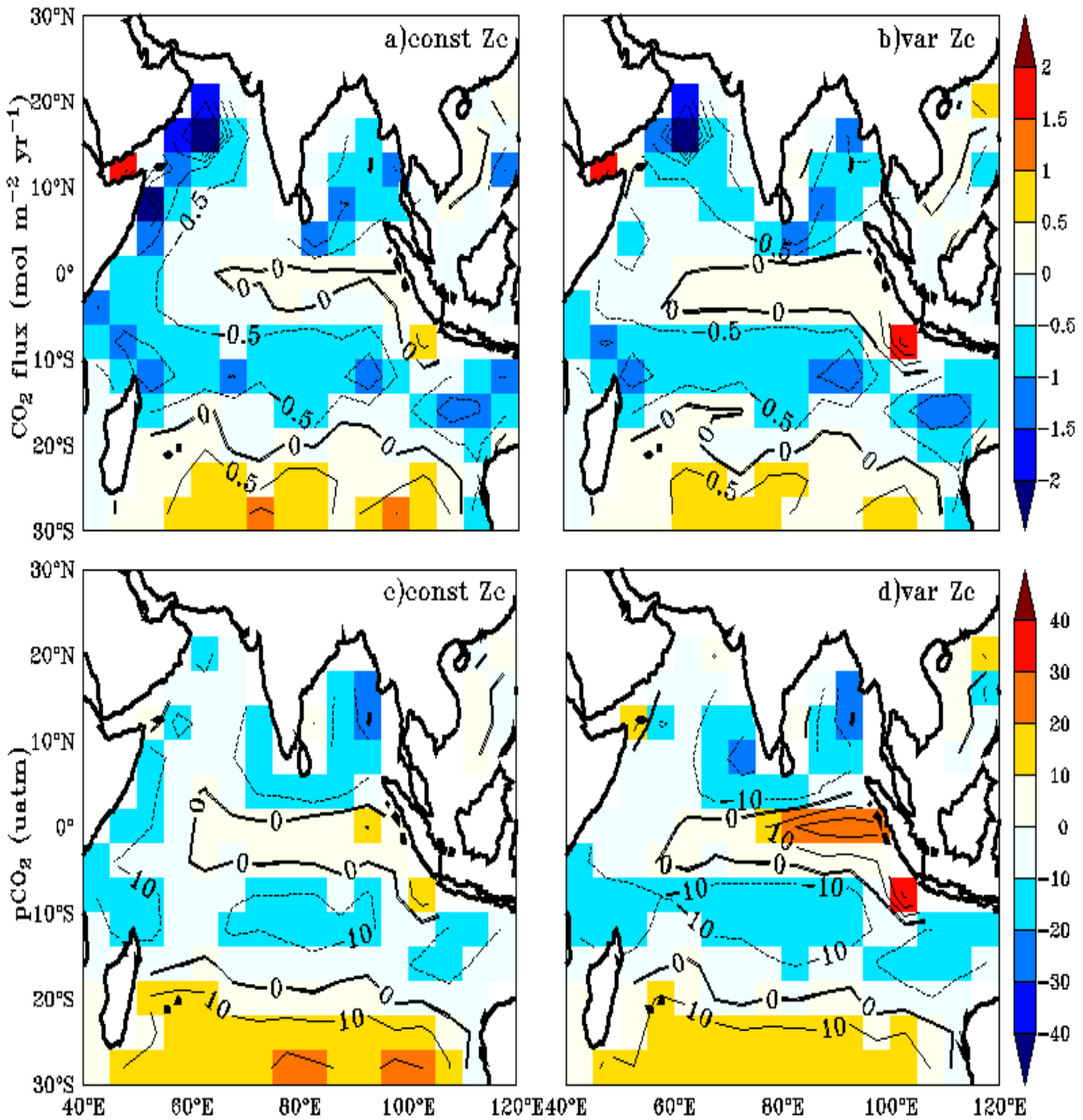
Figure 4: Annual mean biases in the model evaluated against Takahashi et al. (2009) observations for CO_2 flux (a, b) and pCO_2 (c, d) with constant Zc (constZc) and varying Zc (varZc). Units of CO_2 flux and pCO_2 are mol m^{-2} yr^{-1} and μatm, respectively.
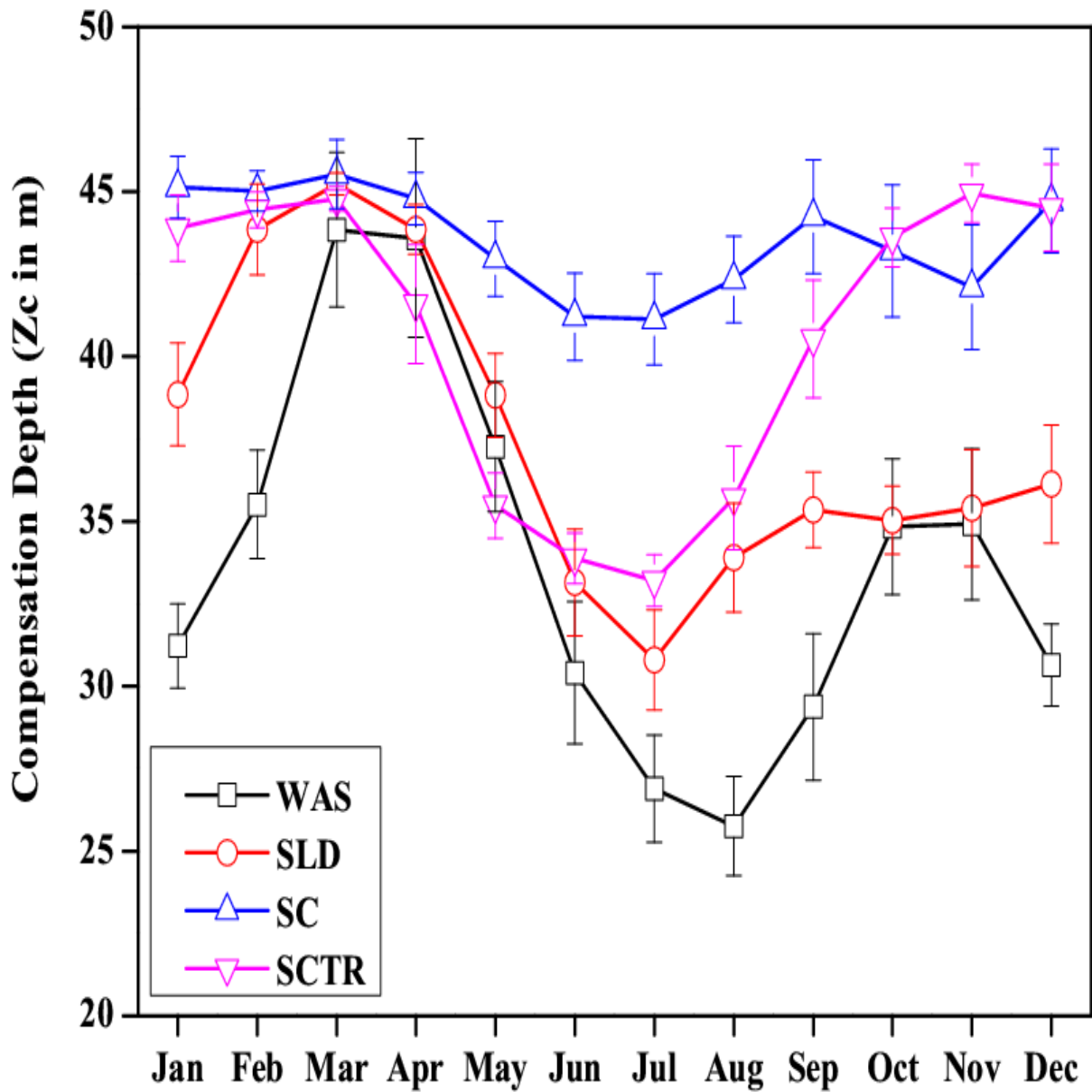
Figure 5: Seasonal variations in varZc over the study regions shown as climatology computed over 1990-2010. Error bar shows standard deviations of individual months over these years. Units are meters.
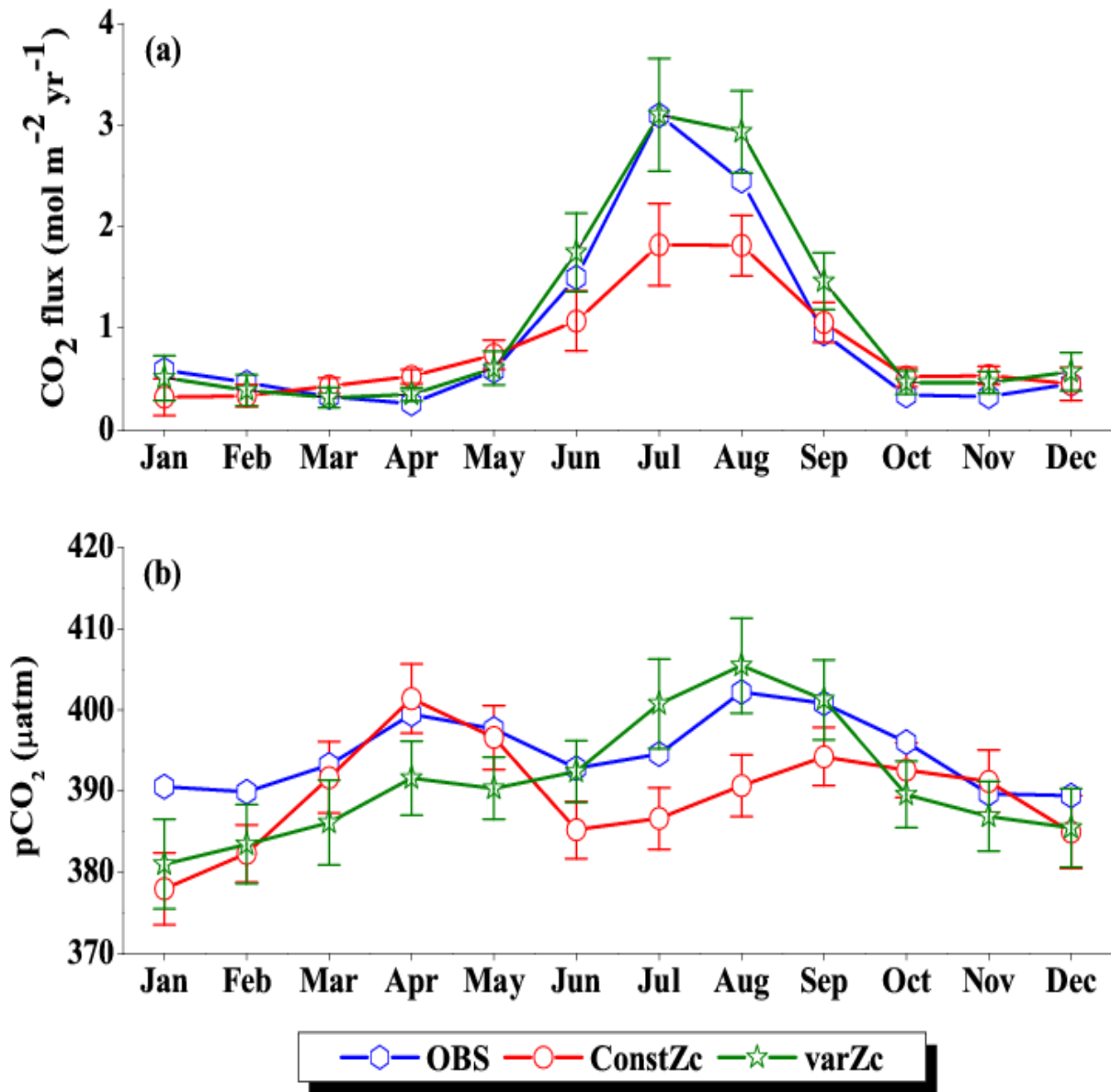
Figure 6: Comparison of model (a) CO_2 flux and (b) pCO_2 simulated with constZc and varZc with that of Takahashi et al. (2009) observations (OBS) over WAS as climatology computed over 1990-2010. Error bar shows standard deviations of individual months over these years. Units of CO_2 flux and pCO_2 are mol m^{-2} yr^{-1} and μatm, respectively. Legend is common for both graphs.
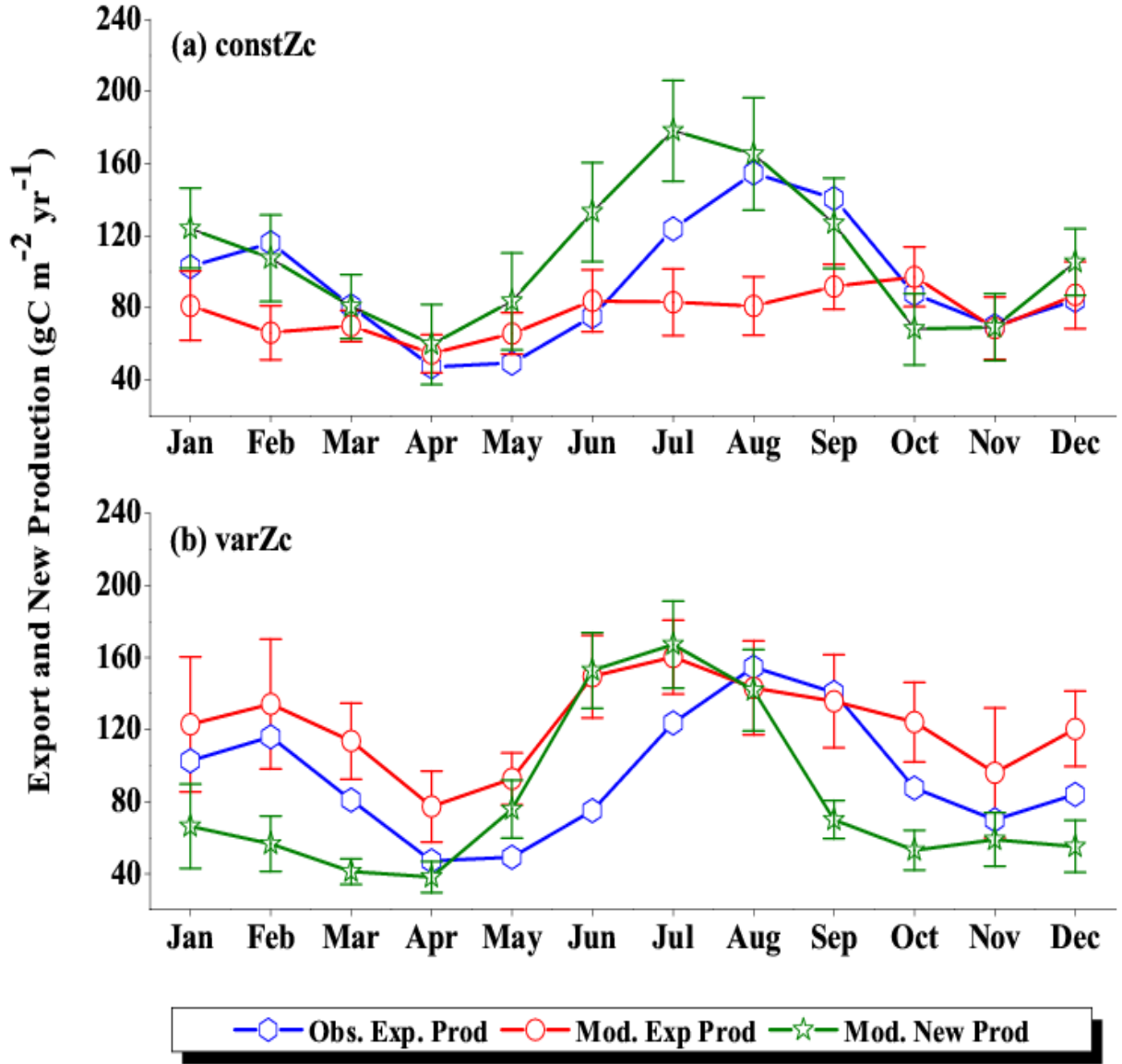
Figure 7: Comparison of model export production (Mod. Exp. Prod) and new production (Mod. New Prod) with satellite-derived export production (Obs. Exp. Prod) for (a) ConstZc and (b) varZc simulations for WAS. Units are g C m^{-2} yr^{-1}. Legends are common for both graphs.
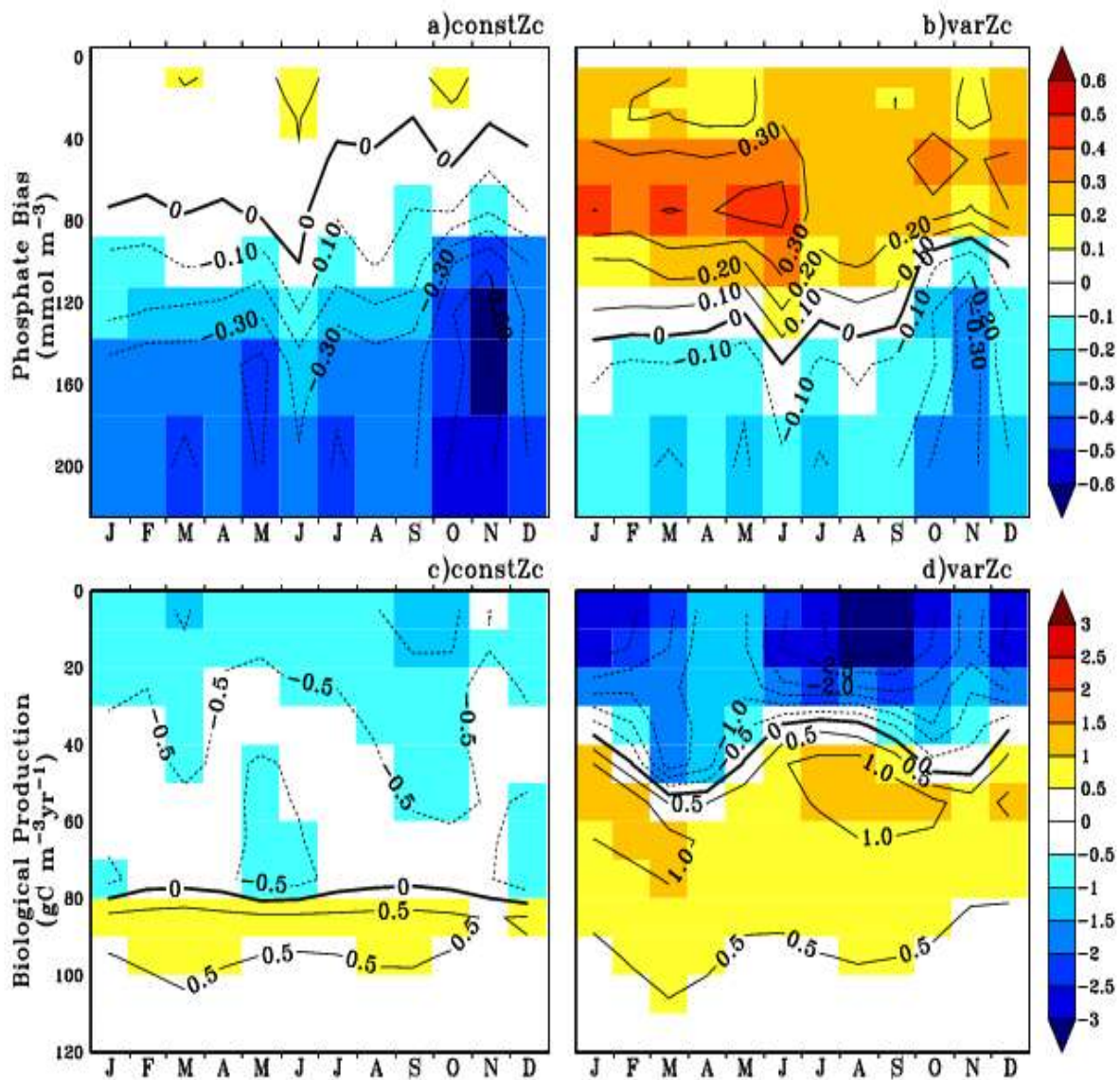
Figure 8: Annual mean bias of model phosphate when compared with climatological observational data (a) for constZc and (b) for varZc simulations. Corresponding annual mean biological source/sink profiles (c, d) in the model for WAS. Unit of phosphate is mmol m^{-3} and biological source/sink is g C m^{-3} yr^{-1}.
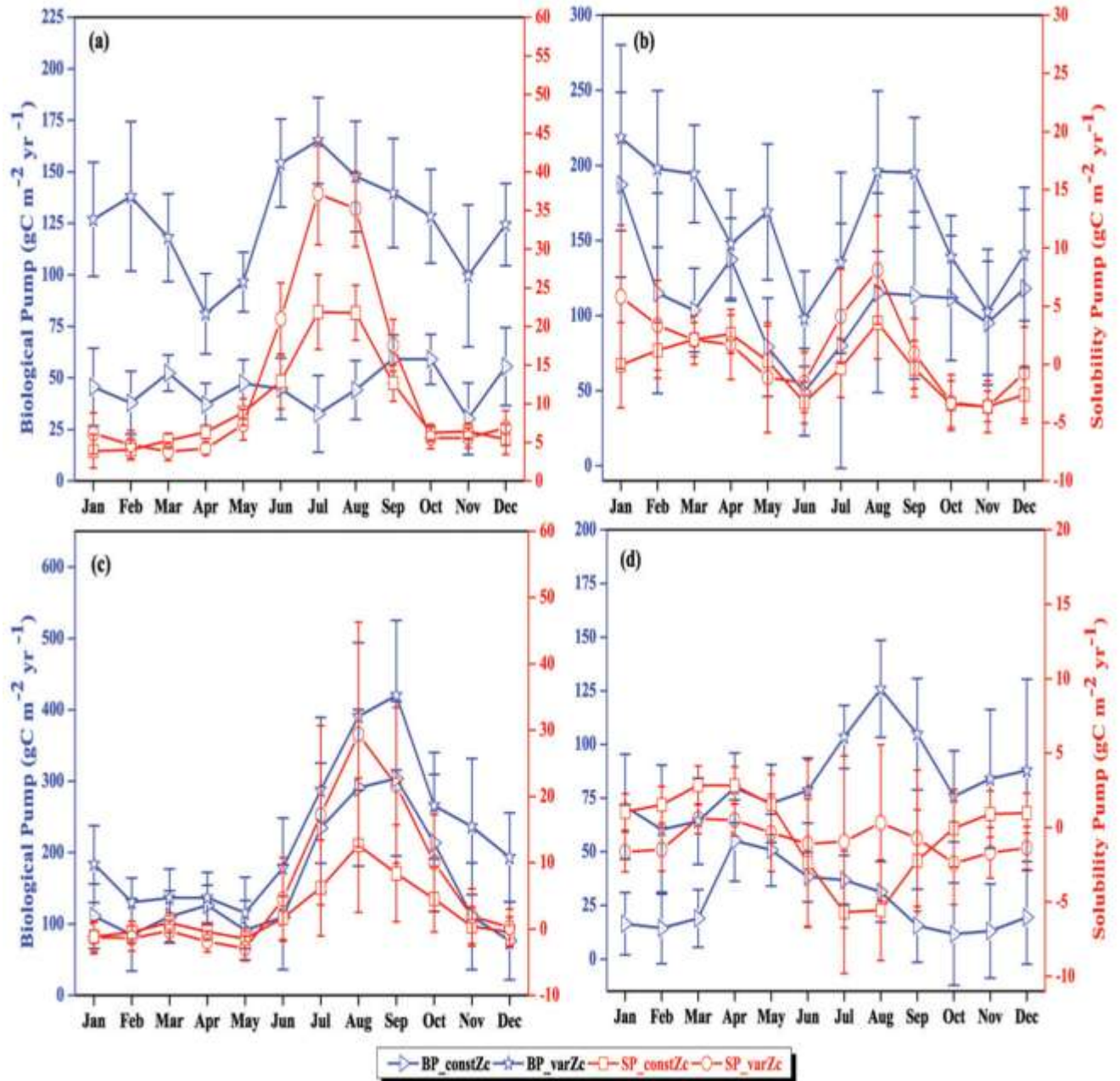
Figure 9: The strength of the biological pump (BP, black lines) and solubility pump (SP, red lines) from constZc and varZc simulations for (a) WAS (b) SLD (c) SC and (d) SCTR. The left axis shows the biological pump and the right axis shows the solubility pump. Error bar shows standard deviations of individual months over the years 1990 - 2010. Units are g C m^{-2} yr^{-1}.
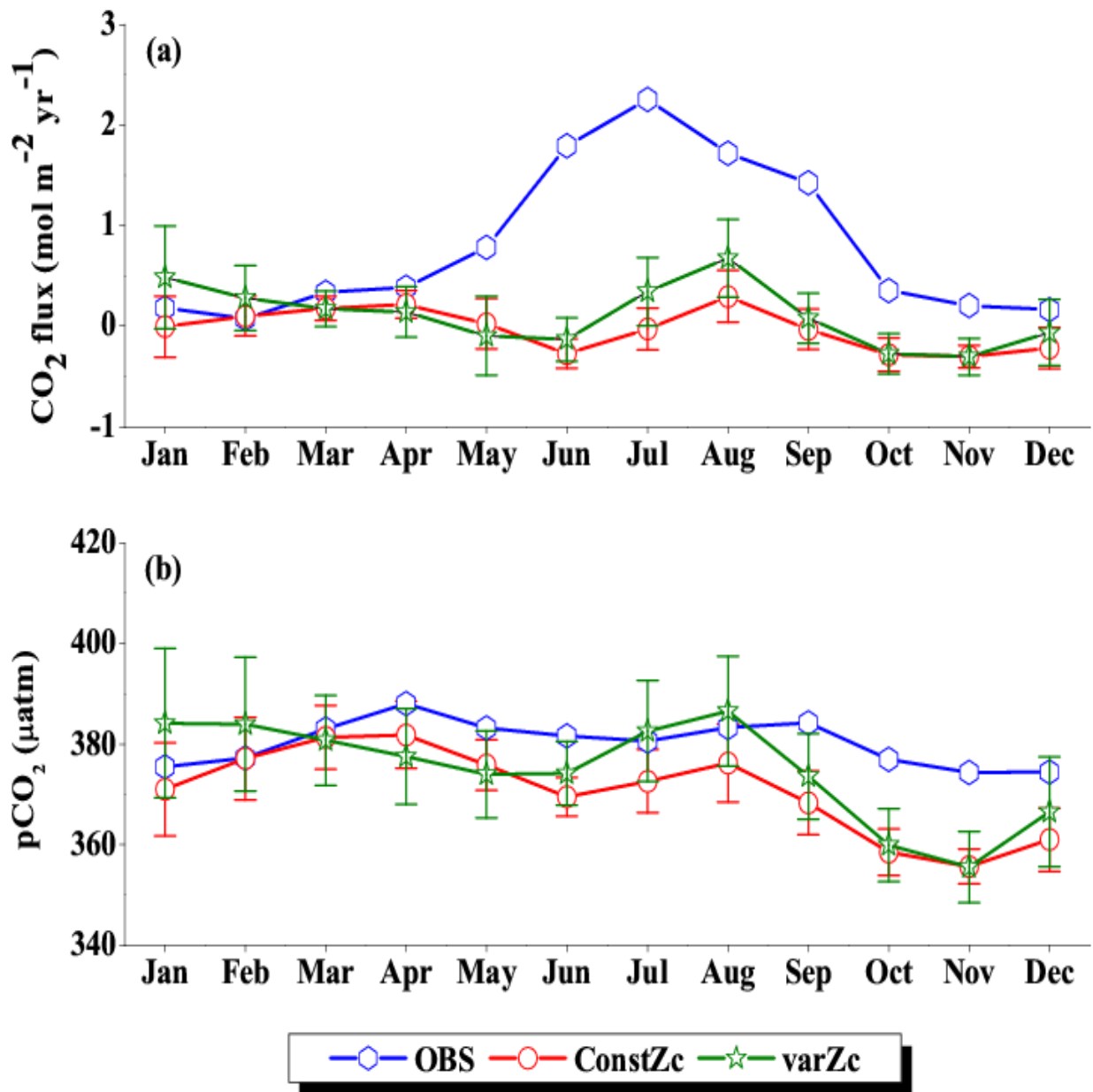
Figure 10: Same as Figure (6), but for SLD.
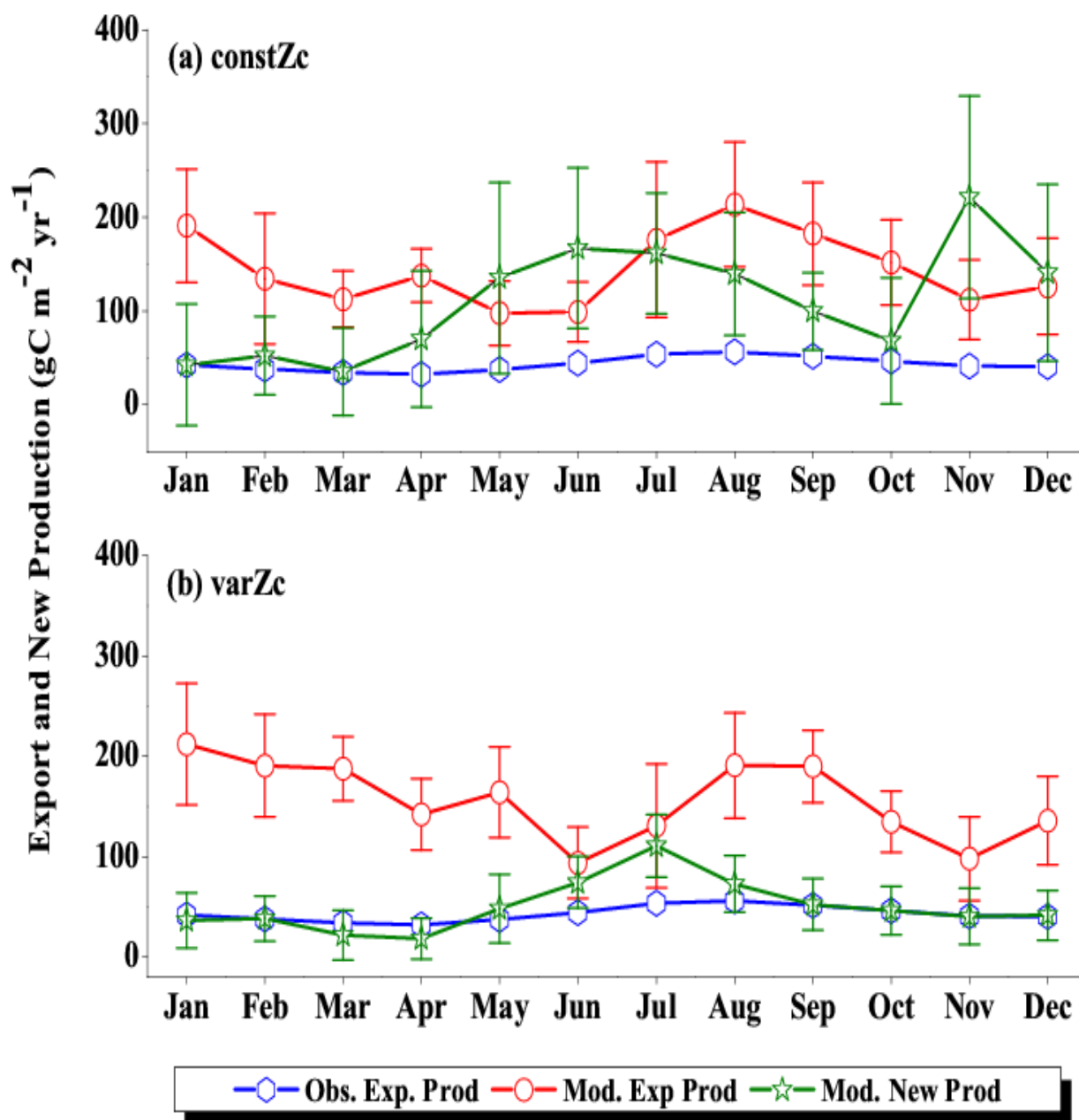
Figure 11: Same as Figure (7), but for SLD.
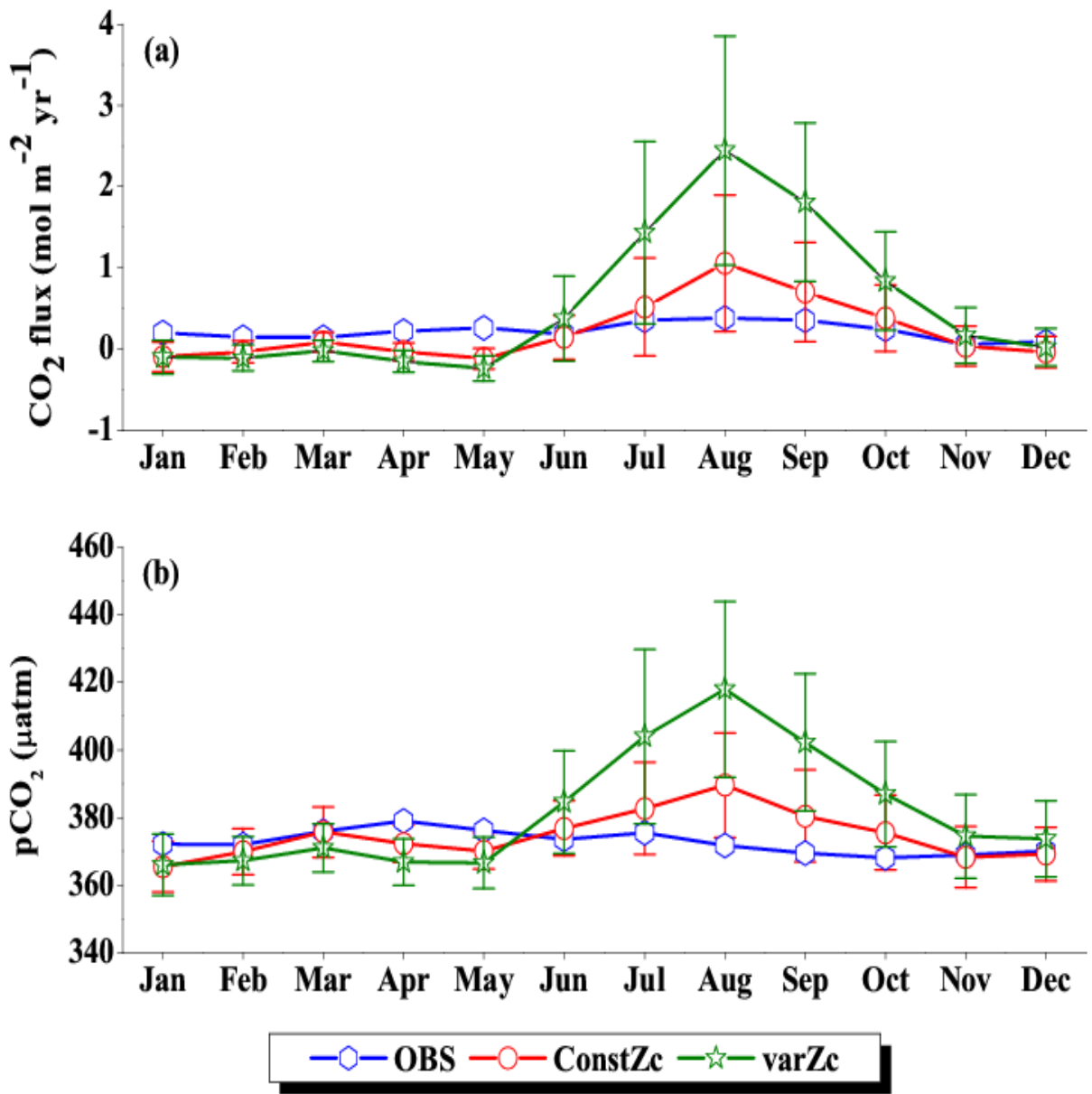
Figure 12: Same as Figure (6), but for SC.
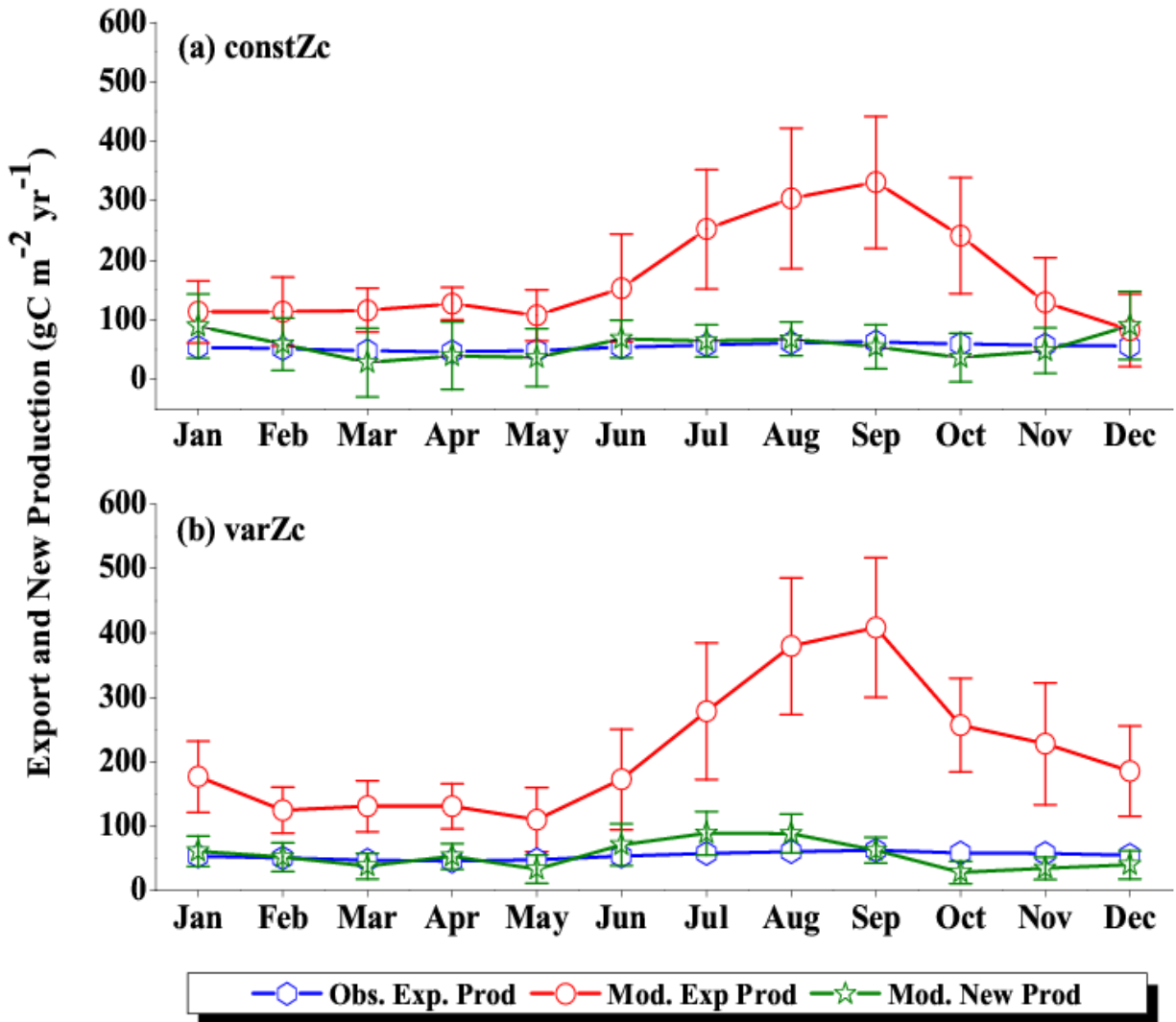
Figure 13: Same as Figure (7), but for SC.
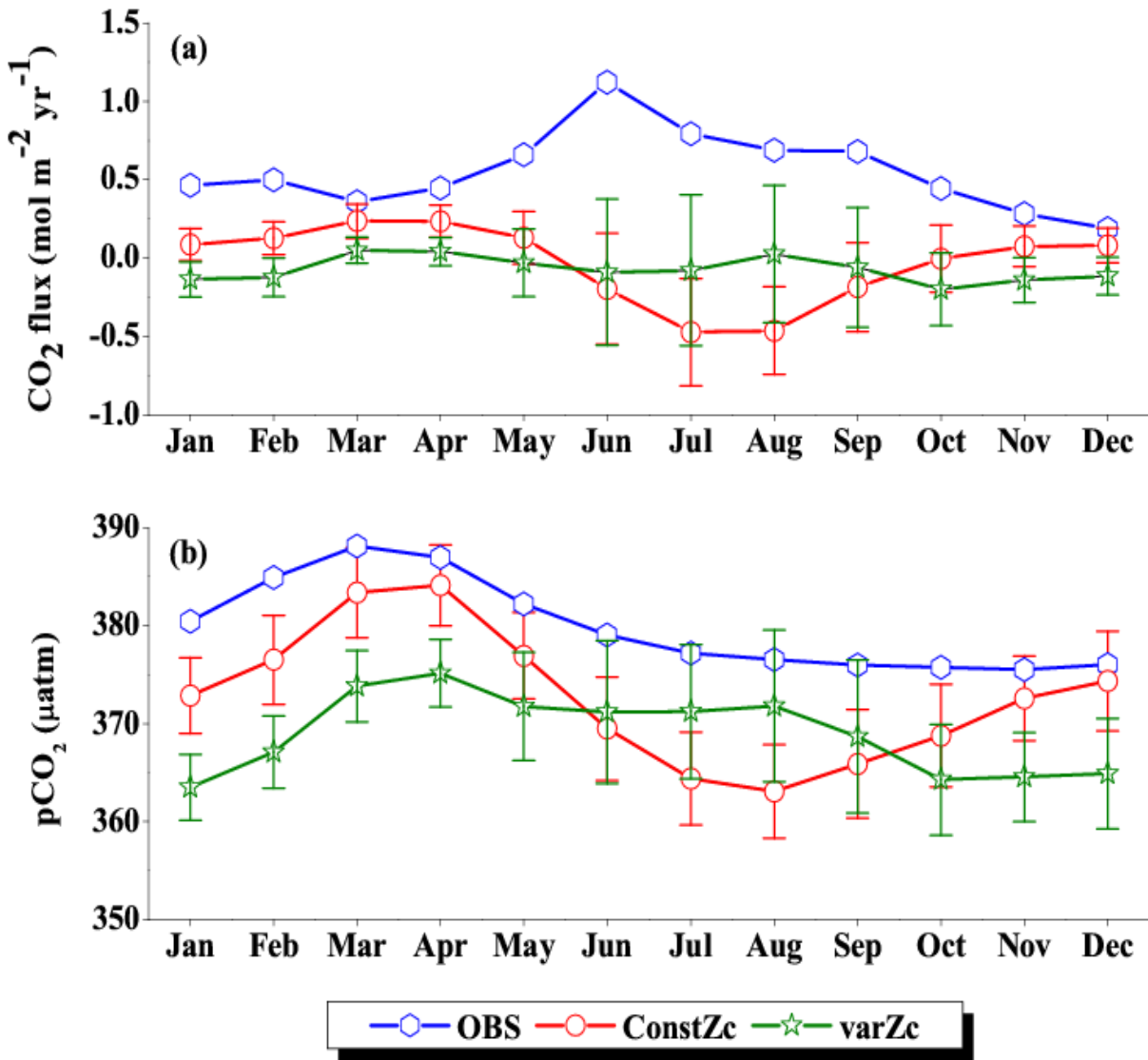
Figure 14: Same as Figure (6), but for SCTR.
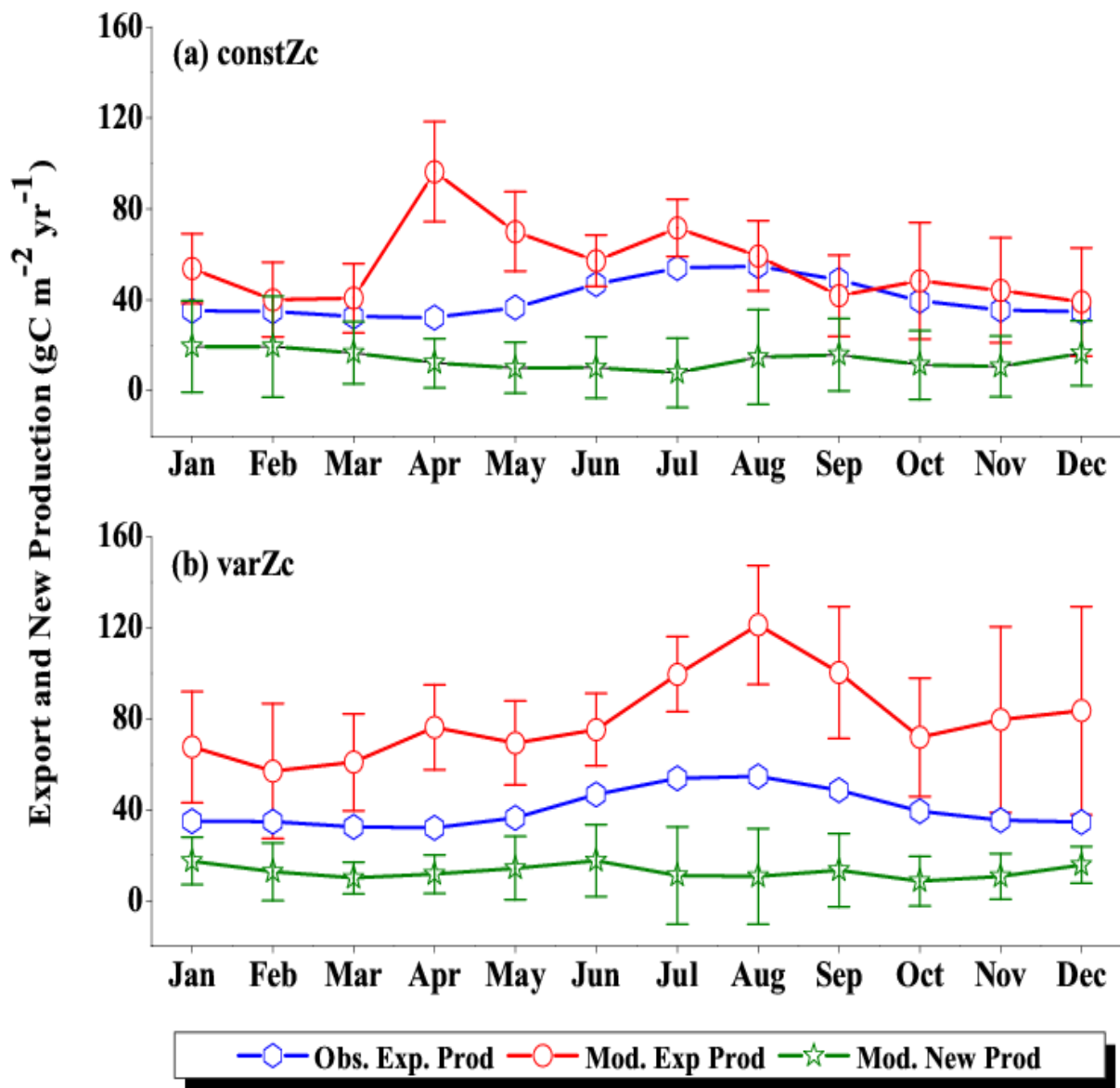
Figure 15: Same as Figure (7), but for SCTR.